Series 07 Aerospace Materials 11

Bonded Repairs for Aircraft Fuselages

A. Vlot/S. Verhoeven/P.J.M. Nijssen

Delft University Press

Bonded Repairs for Aircraft Fuselages

Series 07: Aerospace Materials 11

Bonded Repairs for Aircraft Fuselages

A. Vlot/S. Verhoeven/P.J.M. Nijssen

Delft University Press / 1998

Published and distributed by:

Delft University Press
Mekelweg 4
2628 CD Delft
The Netherlands
Telephone +31 (0)15 278 32 54
Fax +31 (0)15 278 16 61
e-mail: DUP@DUP.TUDelft.NL

by order of:

Faculty of Aerospace Engineering
Delft University of Technology
Kluyverweg 1
P.O. Box 5058
2600 GB Delft
The Netherlands
Telephone +31 (0)15 278 14 55
Fax +31 (0)15 278 18 22
e-mail: Secretariaat@LR.TUDelft.NL
website: http://www.lr.tudelft.nl

Cover: Aerospace Design Studio, 66.5 x 45.5 cm, by:
Fer Hakkaart, Dullenbakkersteeg 3, 2312 HP Leiden, The Netherlands
Tel. +31 (0)71 512 67 25

90-407-1804-0

Printed in The Netherlands

CONTENTS

LIST OF SYMBOLS & ABBREVIATIONS

Symbol	Description	Dimensions
A	area	m^2
A	constant	--
a	half crack length	m
a	ellipse half long axis	m
B	constant	--
B	half overlap length	m
b	debond height	m
b	ellipse half short axis	m
CTE	Coefficient of Thermal Expansion	$^oC^{-1}$
d	diameter	m
da/dN	crack growth rate	mm/cycle
DSA	Damage Source Assignment	--
E	Young's modulus	MPa
e	eccentricity jump	m
FEM	Finite Element Method	--
FML	Fiber Metal Laminate	--
FOD	Foreign Object Damage	--
G	shear modulus	MPa
G	crack extension force	N/m
GAG	Ground-Air-Ground cycle	--
I	second moment of inertia	m^4
K	stress intensity factor	$MPa\sqrt{m}$
LTL	bonded Lap joint load Transfer Length	m
M	moment	Nm
MSD	Multiple Site Damage	--
m	heat transfer coefficient	m^{-1}
N	cycles	--
NLM	Neutral Line Model	--
P	remote stress in x-direction	MPa
P	load per unit length	N/m
Q	remote stress in y-direction	MPa
$\dot{Q}$	heat transfer rate	WK^2
R	radius	m
R	stress ratio	--
r	radial coordinate	m
S	absolute patch separation	m
T	temperature	^oC
t	thickness	m
v	out-of-plane deflection	m
w	separation between neutral line and line of action	m
x	x-coordinate	m
y	y-coordinate	m
z	z-coordinate	m
α	coefficient of thermal expansion	$^oC^{-1}$

ε	strain	--
γ	shear strain	--
Λ^{-1}	bonded lap joint load transfer length	m
ν	Poisson's ratio	--
σ	stress	MPa
τ	shear stress	MPa

sub- and superscripts

A	adhesive
b	bending
bend	bending
c	crack
c	cure
eff	effective
f	force
I	inclusion
long	longitudinal
max	maximum
mid	midsection of repaired skin
min	minimum
op	opening
P	plate
R	repair
r	repaired value
trans	transitional
x	x-direction
y	y-direction
0	undisturbed
γ	shear
∞	infinity

CHAPTER 1

INTRODUCTION

1.1 Background information on bonded repairs

Nowadays, fleet operators tend to use their aircraft longer than intended by their designers out of economical reasons, the original design life is no longer considered to be sufficient. Fatigue problems become an important topic in the maintenance of these aircraft. These so-called "aging aircraft" need safe, damage tolerant and cost-effective repairs. The most recent example emphasizing the need for safe repairs was the Aloha accident. On 28 April 1988, Aloha Airlines Flight 243 (Boeing 737-200) had an explosive decompression in upper cabin area (figure 1.1). The crew was able to execute a successful emergency landing with a significant part of the upper fuselage missing.

Figure 1.1: The Aloha Airlines Boeing 737-200 after the accident

Research revealed a fundamental problem called "multiple site damage" (MSD). Multiple site damage typically consists of a large number of cracks, mostly originating at the edges of adjacent and collinear fastener holes, lap joints, etc. In the case of the Aloha aircraft, multiple small fatigue cracks in the longitudinal riveted joints in the aluminum skin of the aircraft were found. A more or less uniform stress field is required for MSD and this makes MSD almost unlikely to occur in wings, it usually occurs in longitudinal skin splices of a pressurized fuselage structure.

As mentioned before, multiple site damage is a severe problem for aging aircraft but certainly not the only problem, other problems are for example corrosion and impact damage. To illustrate the problem: by the year 2000, more than 5700 commercial aircraft will be over twenty years old. As of 1993, 51% of the United States Air Force (USAF) fleet was over fifteen years in age and 44% of the USAF fleet was over twenty years in age [1.1]. This requires a method to restore the desired fatigue life of these aging aircraft.

1.2 Repair methods: bonded vs. riveted repairs

In general, the highest cost of a repair will be downtime and labor. The best available repair method will decrease downtime of the aircraft in future operations and will also provide the safest way of operating the aircraft. There are three options to restore the original strength of a cracked structure:

- Re-skinning of the cracked structure
- The traditional method: riveting patches over the cracked structure
- Application of adhesively bonded repairs

Repairing a cracked or corroded fuselage skin can be a good alternative for re-skinning when both economical and technical benefits can be achieved. In general, when it is possible to use riveted or bonded repairs, re-skinning is a financially unattractive option.

Conventional repairs for thin-skinned structures are riveted monolithic aluminum sheets. For the last decades this has been the main method for repairing fuselage cracks. First, the crack is stop-drilled or completely removed by drilling a larger hole. This hole is covered by an aluminum plate, which is riveted to the skin. In principle, the main advantage of a mechanically fastened (i.e. riveted) joint, is the fact that they can be subsequently disassembled and that the application can be done in an uncontrolled environment. Another advantage of riveting is that it is easy to carry out and it requires little support equipment.

On the other hand, methods based on mechanical fastening can result in considerable damage to the parent structure [1.2], for example:

- Additional fastener holes introduce stress concentrations and thus possible new fatigue-critical locations. Consequently, the inspection requirements have to be increased, resulting in higher costs.
- In-situ drilling may cause internal damage to items such as hydraulic lines and electrical wiring.
- Poor mechanical fastening procedures may result in fretting damage, encouraging stress-corrosion cracking.
- Loss of rivets on an outside surface repair, due to mechanical working of the fastened region, may result in FOD to engines.

For many applications, instead of riveted repairs, bonded repairs might be an alternative. Compared to mechanical fastening such as riveting or bolting, adhesive bonding provides more uniform and efficient load transfer into the patch and can reduce the risk of high stress concentrations. Adhesively bonded repairs can also be removed without causing significant damage to the structure.

However, the necessary and stringent cleaning and processing steps restrict the use of bonded joints. The use of an adhesive requires application in a controlled environment. Surface cleaning should be done away from any contaminating operations, such as dust generating operations (sanding, grinding, etc.). Next to that, adhesively bonded joints must be designed in a way that the adhesive is loaded in the direction of maximum strength (shear). Tensile and peel stresses should be avoided or minimized.

The first successful application of an advanced composite in a bonded repair was done in 1969, when composite patches were applied to the fracture-critical D6AC steel wing pivot fitting of the General Dynamics F-111 by the former Aeronautical Research Laboratories and the Royal Australian Air Force [1.3]. Within the US Department of Defense, notable success stories include the C-141B and the C-5A transport aircraft, the F-111 and F-16 fighter-bombers and the B-1B strategic bomber. By now, the military has successfully used boron/epoxy patches for over 20 years and more than 6,500 boron patches are flying today. Commercial use is in the introductory phase, with about 250 patches flying [1.4]. Adhesively bonded repairs have shown to be a highly efficient and cost effective method, significant increases in fatigue life can be achieved (see figure 1.2).

As a rule, adhesive joints prove to be most efficient for lightly loaded structures, while mechanically fastened joints are more efficient for highly loaded structures. In general, bond line imperfections, such as voids and porosity, result in a reduction in the thickness of members that can be bonded satisfactorily. For thick fail safe structures, bond flaws must be avoided as they can propagate catastrophically. Kelly [1.5]: "It is best to restrict the use of adhesive bonding to those applications and designs in which there is no possibility of any local bond flaw growing during the life of the aircraft and it is unwise to ever design or build a purely bonded joint which is weaker than the members themselves."

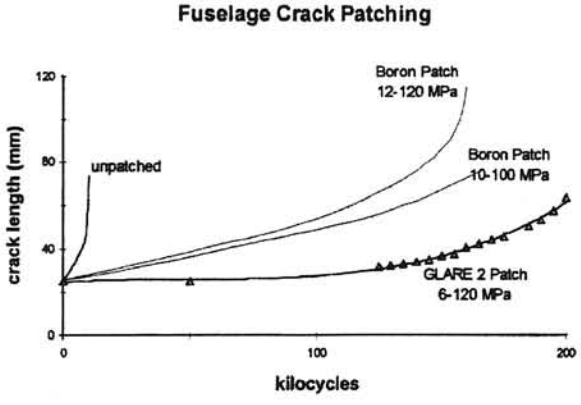

Figure 1.2: Crack growth rates for a few bonded repair configurations [1.6]

The outline of this report is as follows. Chapter 2 will give a short description of design and analyses methods that are available. Chapter 3 will give an overview of the processes and materials involved in the field of bonded repairs. These two introductory chapters are followed by chapters that will describe the work that has been performed at the Faculty of Aerospace Engineering of Delft University of Technology. Chapter 4 will give a description of the bonded repair analysis program CalcuRep®, developed in cooperation with the United States Air Force Academy. In chapter 5, the results of calculations of stress intensity factors and stresses in the periphery of bonded repairs are given, using FEM and the Neutral Line Model. Chapter 6 will show some results of in-service effects on bonded repair efficiency and finally, chapter 7, will describe the application and qualification of a bonded GLARE® repair on a C-5A Galaxy cargo aircraft.

[1.1] Denney, J.J., Mall, S., *Effect of Disbond on Fatigue Behaviour of Cracked Aluminium Panel with Bonded Composite Patch,* Department of Aeronautics and Astronautics, Air Force Institute of Technology, Wright-Patterson AFB OH.

[1.2] Baker, A.A., "Crack Patching: experimental studies, practical applications" in: Baker, A.A., Jones, R., editors, *Bonded Repair of Aircraft Structures,* pp. 107-173, Martinus Nijhoff Publishers, Dordrecht, The Netherlands, 1988.

[1.3] Baker, A. A., *Bonded Composite Repair of Metallic Aircraft Components - Overview of Australian activities,* Proceedings of the 1994 AGARD specialists' meeting on composite repair of military aircraft structures, Seville, Spain, October 1994, AGARD-CP-550.

[1.4] http://www.minmet.mcgill.ca/~metsoc/Ageair.htm

[1.5] Kelly, L.J., "Introductory Chapter" in: Baker, A.A., Jones, R., editors, *Bonded Repair of Aircraft Structures,* pp. 3-18, Martinus Nijhoff Publishers, Dordrecht, The Netherlands, 1988.

[1.6] Guijt, C.B., Fredell, R.S., *Delamination Effects in Fuselage Crack Patching,* Proceedings of the 41st International SAMPE symposium, 1996.

CHAPTER 2

DESIGN AND ANALYSIS METHODS FOR BONDED REPAIRS

2.1 Introduction

Several computer codes for design and analysis of bonded repairs are being developed around the world. The stress analysis of an adhesively bonded repair is usually based on two different methods:

- Analytical analysis
- Finite element modeling (FEM)

FEM analysis requires a considerable amount of modeling and computing efforts since a very fine mesh must be used near the crack tips due to the presence of stress singularities. Some adaptations to conventional finite element methods have been made to improve the efficiency and accuracy (see e.g. [2.1]). Examples of some FEM modeling can be found in chapter 5 and in [2.2] and [2.3].

Analytical analysis of bonded repairs started in the early seventies. The models that are currently used are mainly based on the so-called Rose model. Other research [2.4/2.5] involved an infinite composite patch, adhesively bonded to an infinite cracked unstiffened sheet. The adhesive was treated as 2-dimensional shear springs. The problem was reduced to a pair of integral equations that was solved by numerical integration with the discretisation of the bonded interface. The size of the debond was determined by calculating the shear strain in the adhesive and comparing these values with the allowable shear strain in the adhesive. Ratwani and Kan [2.6] considered extension of these models to complex repair situations. However, these problems were not solved analytically and results might be inaccurate [2.7].

2.2 The Rose model

This section describes the mathematical background necessary for the analysis of bonded repairs. The basic theory was developed by L.R.F. Rose. The Rose model covers the stress intensity solution, K, for the repaired crack, the adhesive shear strain in the bond line and the load attraction into the stiffened area. The Rose model is a continuum analysis based on the theory of elasticity. It considers an infinitely wide center-cracked isotropic plate with a one-

sided bonded orthotropic elliptical patch. The plate is remotely loaded by a bi-axial stress system.

The analysis is divided into two parts. In stage 1, the repair is analyzed without a crack and modeled as an equivalent inclusion. The objective of stage 1 is to calculate the stress redistribution in the plate due to the presence of the bonded doubler. Stage 2 introduces the crack and the crack faces become stress free. The stress intensity factor at the crack tip can be determined, using the results of stage 1.

The Rose model also takes the effects of thermal residual stresses due to curing and operating temperature into account. The different stages can be seen in figure 2.1 through 2.3.

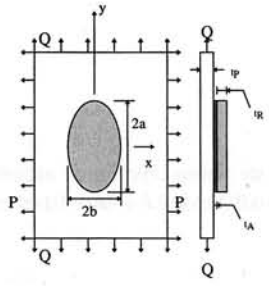

Figure 2.1: Stage I of the Rose model (bonded patch, no crack, no out-of-plane displacements)

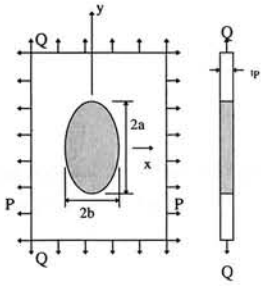

Figure 2.2: Stage I of the Rose model (no crack, equivalent inclusion representing plate and patch)

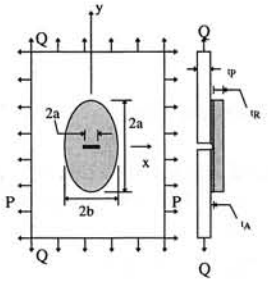

Figure 2.3: Stage II of the Rose model (crack introduced)

The patch has an elliptical shape in order to be able to use an analytical solution. Next to that, an ellipse is an efficient shape for load transfer in an adhesive. Rectangular patches, preferred in riveted repairs and used in some bonded repairs, can result in high peel stresses at the patch corners which can result in debond growth, typically resulting in an elliptical bond line.

Load transfer in bonded joints

Before this two-stage model can be used, an analysis of the load transfer from the plate into the patch has to be made. This analysis is based on the one-dimensional analysis of load transfer in bonded joints by Hart-Smith [2.8].

There are two areas of interest. The first area is the load transfer zone at the patch edge, the second area is the load transfer zone around the crack. The shear stresses are highest in these two transfer zones. In order to allow the assumptions, which are necessary for the Rose model (see next paragraph), the load transfer length (LTL) has to be small for both zones.

In Hart-Smith's analysis, the adhesive layer is treated as an adhesive shear spring. Each adherend is treated as a one-dimensional continuum whit a deformation that is specified by the longitudinal displacement and stress.

The shear traction, exerted by the adhesive, can be replaced by an equivalent body force, which is distributed uniformly across the thickness of each adherend. This leads to the following differential equation:

$$\tau_A''(y) - \Lambda^2 \tau_A(y) = 0 \qquad (2.1)$$

With the characteristic quantity *LTL* defined as :

$$LTL = \frac{1}{\Lambda} \text{ where } \frac{1}{\Lambda} = \left(\frac{t_A}{G_A} \left[\frac{E_{xP} t_P E_{xR} t_R}{E_{xP} t_P + E_{xR} t_R} \right] \right)^{1/2} \qquad (2.2)$$

where t_A is the adhesive thickness (mm),
t_P is the plate thickness (mm),
t_R is the reinforcement (patch) thickness (mm),
E_{xP} is the elastic modulus of the plate in the x-direction (GPa),
E_{xR} is the elastic modulus of the reinforcing patch, x-direction, and where
G_A is the adhesive shear modulus (MPa).

For a typical aluminum alloy skin thickness and epoxy film adhesives, this transfer length is in the order of three to seven millimeters.

The solution for differential equation 2.1 is an exponential function and is defined as:

$$\tau_A(y) = \frac{F}{E_P t_P} \frac{G_A}{t_A} \frac{\sinh(\Lambda y)}{\Lambda \cosh(\Lambda B)} \qquad (2.3)$$

where B is defined as the half overlap length.

This function describes the magnitude of the shear stresses in the bond line. These shear stresses decay exponentially from the overlap ends. A similar analysis is made for the region around the crack. However, in real-life repairs, the adhesive shear stresses at the crack flank are somewhat higher than at the overlap ends. This is due to the tapering at the patch edge to reduce adhesive peel and shear stresses and substrate bending stresses.

Stage I: Inclusion analogy

The Rose analysis is based on the following assumptions:

- All materials are modeled linear elastic, except for limited elastic-plastic deformation in the adhesive near the crack.
- All plate and patch materials are in a state of generalized plane stress. No through-the-thickness variation occurs in the basic analysis. This assumption is valid for thin structures but can be unconservative for a one-sided repair on a thick cracked structure. Thus when no bending occurs, normal stresses will be constant throughout the thickness of the plate and patch. Additional bending stresses will result in a linear stress distribution throughout the thickness.

- The adhesive layer behaves as a linear shear spring, except for limited elastic-plastic deformation in the adhesive layer near the crack.
- The basic model ignores thermal stresses due to curing and operating temperatures.
- Bending along the crack, caused by a shift in neutral axis due to a one-sided patch, is restrained by the substructure. This assumption is considered reasonable since fatigue damage occurs in most cases at lap joints, frame connections etc.

In this part of the analysis, the main objective is to calculate the stresses in the plate after the stress redistribution due to bonding of the patch to the plate. This is done by modeling the patch and the plate underneath the patch as one elastic inclusion in the plate (see figure 2.2). This analogy was first formulated by Muki and Sternberg [2.9] and expanded by Rose [2.10]. First, the elastic constants of this inclusion have to be determined, as was done by Rose [2.11] and Fredell [2.12].

Consider the repair configuration shown in figure 2.1, loaded by the following remote bi-axial stress:

$$\sigma_x = P, \qquad \sigma_y = Q, \qquad \tau_{xy} = 0 \tag{2.4}$$

Equilibrium in the inclusion implies:

$$t_I \sigma_{xI} = t_P \sigma_{xP} + t_R \sigma_{xR} \tag{2.5}$$

Another result of the locally increased stiffness is load attraction into the repaired area. These local increments in stresses are denoted by p and q, in the x-and y-directions, respectively. It can be derived that the stresses within the elliptical inclusion are homogeneous.

The derivations of the equations for the stresses in the plate and patch are presented in [2.13]. The stresses in the equivalent inclusion are represented in final form by:

$$\sigma_{xI} = P + p, \quad \sigma_{yI} = Q + q, \quad \tau_{xyI} = 0 \tag{2.6}$$

With Lekhnitskii's inclusion analysis [2.14], a set of linear equations for p an q is obtained. The equations derived for the present case are valid for isotropic skin material only. The following set of equations can be derived:

$$\left\{\begin{array}{l} \left[\frac{b}{a}\frac{2}{E_{xP}} + \frac{1}{E_{xI}}\right]p - \left[\frac{1-\nu_P}{E_{xP}} + \frac{\nu_I}{E_{xI}}\right]q = \left[\frac{1}{E_{xP}} - \frac{1}{E_{xI}}\right]P - \left[\frac{\nu_P}{E_{xP}} - \frac{\nu_I}{E_{xI}}\right]Q \\ -\left[\frac{1}{E_{yP}} - \frac{\nu_P}{E_{xP}} + \frac{\nu_I}{E_{xI}}\right]p + \left[\frac{a}{b}\frac{2}{E_{yP}} + \frac{1}{E_{yI}}\right]q = -\left[\frac{\nu_P}{E_{xP}} - \frac{\nu_I}{E_{xI}}\right]P + \left[\frac{1}{E_{yP}} - \frac{1}{E_{yI}}\right]Q \end{array}\right\} \tag{2.7}$$

With equation 2.7 the undisturbed stress in the panel and repair can be calculated:

$$\sigma_{xP} = \sigma_{xI}\left[1 - \frac{t_R}{t_I}\frac{(A_{xR} - \nu_I \nu_R A_{yR})}{E_{xI}}\right] + \sigma_{yI}\frac{t_R}{t_I}\left[\frac{\nu_I}{E_{xI}}A_{xR} - \frac{\nu_R}{E_{yI}}A_{yR}\right] \tag{2.8}$$

Rearrangement of equation 2.5 gives:

$$\sigma_{xR} = \frac{t_I}{t_R}\sigma_{xI} - \frac{t_P}{t_R}\sigma_{xP} \tag{2.9}$$

Analogous expressions are given for σ_{yP} and σ_{yR} in [2.13]. At the patch tip, the load in the inclusion in the load direction is completely carried by the skin. This yields a simple boundary condition for the tip stress, the highest stress adjacent to the patch:

$$\begin{aligned} t_P\sigma_{xP} = t_I\sigma_{xI} \Rightarrow \sigma_{xP} = \sigma_{xI}\frac{t_I}{t_P} \\ t_P\sigma_{yP} = t_I\sigma_{yI} \Rightarrow \sigma_{yP} = \sigma_{yI}\frac{t_I}{t_P} \end{aligned} \tag{2.10}$$

The effect of an elastic inclusion on the "load flow" is illustrated by the stress trajectories shown in figure 2.4 for a stiff inclusion.

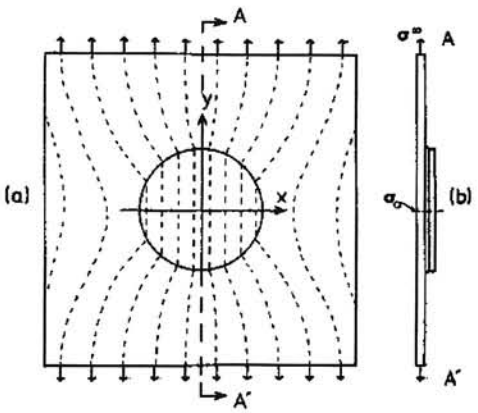

Figure 2.4: Idealized "load flow" into elliptical reinforced region of plate [2.11]

Stage II: Introduction of the crack

In stage II, a crack of length $2a_c$ is introduced in the plate along the line y = 0. The rigid bond assumption no longer applies and forces along the crack face are relaxed to zero. The patch is assumed to completely cover the crack in stage II to make the calculation of the repaired stress intensity factor K_r possible.

The stage I plate stress σ_{xP} was denoted σ_0 to signify the (constant) plate stress in the inclusion. However, the introduction of the crack in stage II causes the forces in the vicinity to be redistributed. Some of the load is transferred into the patch while the remainder is redistributed around the crack tips.

For effective crack bridging by the patch, a minimum crack length must be reached. Marissen [2.15] and Roebroeks [2.16] and co-workers have reported a similar phenomenon for the fatigue behavior of fiber metal laminates (FMLs), which might be considered cracks that are patched from the inside. Fortunately, the required crack length is rather small, less than 10 mm for typical aircraft structures. In fiber metal laminates, this minimum crack length is much smaller because of the very thin aluminum sheets used. Often, the minimum crack size will be reached or exceeded before inspectors are able to locate it for repair.

The calculation of the repaired stress intensity factor, K_r, for a patched isotropic plate will be given here. The orthotropic case is given in [2.12]. To begin, the crack extension force G_f is defined from linear elastic fracture mechanics:

$$G_f = \frac{K^2}{E} \tag{2.11}$$

This relation can be used to find the boundaries for K between short and long cracks. The crack extension force for a semi-infinite crack is derived from the energy change (per unit width) when going from the configuration in figure 2.1 to figure 2.3. With short cracks, the influence of the reinforcement can be neglected. The short crack stress intensity factor, denoted by K_u, is:

$$K_u = \sigma_o \sqrt{\pi a_c} \tag{2.12}$$

which represents an upper bound for K. For longer cracks, K and G_f are limited by the crack-closing influence of the reinforcement. An expression for the limiting value of the crack extension force G_{f_∞} relies on the assumption that plate and repair are of infinite extent.

The expression for the crack extension force for long cracks is given by (see appendix B of [2.12]):

$$G_{f_\infty} = \frac{t_A}{G_A} \Lambda \sigma_0^{\,2} t_P \tag{2.13}$$

The transition between "short" and "long" cracks can be established by solving for the point where the unpatched value $G_u = G_\infty$. For the isotropic case, this yields a transitional crack length, denoted $a_{c_{trans}}$:

$$a_{c_{trans}} = E_P t_P \frac{t_A}{G_A} \frac{\Lambda}{\pi} \tag{2.14}$$

Thus, for short cracks, the upper bound of K is defined by equation 2.12 while for infinitely long cracks, K is represented by:

$$K_{\infty} = \sigma_o \sqrt{\pi a_{c_{trans}}} \tag{2.15}$$

This was first formulated by Rose [2.13]. An interpolated expression for the repaired value K_r can be written as:

$$K_r = \sigma_o \sqrt{\frac{\pi a_{c_{trans}} a_c}{a_{c_{trans}} + a_c}} \tag{2.16}$$

Equations 2.12, 2.15 and 2.16 are summarized graphically in figure 2.5. For thin structures with an adhesively bonded repair, a_c is typically about 3 mm, therefore it is legitimate that K can be assumed to be constant, as is shown in figure 2.5.

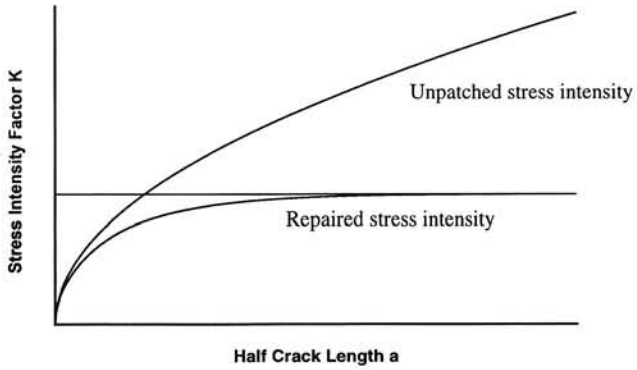

Figure 2.5: Comparison of patched and unpatched K values

Next item to be calculated is the maximum normal stress in the patch. The maximum reinforcement stress occurs at x = 0, y = 0. A conservative estimate is that the entire load in that area of the inclusion is carried by the patch (recall the assumption that no bending occurs across the crack face due to the presence of a stiffener).

$$\sigma_{yR_{max}} \approx \sigma_{yl} \frac{t_P}{t_R} \tag{2.17}$$

Next to the maximum stress in the patch, the maximum strain in the adhesive is of primary interest. The critical adhesive shear strain occurs at the crack face and at the patch tips if they are not tapered.

Using the one-dimensional theory of bonded joints and two-step elastic-plastic analysis yields:

- elastic adhesive behavior: $\sigma_o \Lambda t_P < \tau_{yield}$

Substitution of x = 0 into equation 7 in Appendix B of [2.12] allows solution for the maximum shear strain in the adhesive:

$$\gamma_{max} = \frac{\sigma_o \Lambda t_P}{G_A} \tag{2.18}$$

- plastic adhesive behavior: $\sigma_o \Lambda t_P > \tau_{yield}$

$$\gamma_{max} = \frac{\tau_{yield}}{2G_A}\left[1+\left(\frac{\sigma_o \Lambda t_P}{\tau_{yield}}\right)^2\right] \tag{2.19}$$

In this case, the characteristic crack length $a_{c_{trans}}$ must be modified to:

$$a_c = \frac{E_P t_A}{G_A \pi}\left[\frac{\tau_{yield}}{\sigma_0}\left(1+\frac{\sigma_0 \Lambda t_P}{\tau_{yield}}\right)-\frac{\tau_{yield}^2}{3\Lambda t_P \sigma_0^2}\left(1+2\left(\frac{\sigma_0 \Lambda t_P}{\tau_{yield}}\right)^3\right)\right] \tag{2.20}$$

The strain behavior described by equations 2.19 and 2.20 is presented in chapter 5 of [2.12] for typical toughened structural epoxy adhesives. The maximum adhesive shear strain is plotted versus the nominal gross stress in the adherends of a single lap joint. A stiffer adhesive exhibits less strain than a flexible (toughened) adhesive. However, the stiffer adhesive also reaches its yield point at a much lower adherend normal stress. This performance influences the choice of an appropriate adhesive for a bonded repair. While a stiffer adhesive might be preferable from a crack closing standpoint, adhesive strain levels should be kept below the yield point for good long-term durability. These effects and many other trends are discussed in [2.12].

[2.1] Nagaswamy, V., Pipkins, D.S., Atluri, S.N., *An FEAM Based Methodology for Analysing Composite Patch Repairs of Metallic Structures*, Computer Modeling and Simulation in Engineering, Volume 1, 1996.

[2.2] Tarn, J., Shek, K., *Analysis of Cracked Plates with a Bonded Patch*, Engineering Fracture Mechanics, Volume 40, No. 6, pp. 1055-1065, 1991.

[2.3] Ratwani, M.M., *Characterization of Fatigue Crack Growth in Bonded Structures, Volume II: Analysis of Cracked Bonded Structures*, Final Report, AFFDL-TR-77-31, Air Force Flight Dynamics Laboratory, Wright-Patterson AFB OH, June 1977.

[2.4] Erdogan, F., Arin, K., *A Sandwich Plate with a Part-through and a Debonding Crack*, Engineering Fracture Mechanics, Volume 4, pp. 449-458, 1972.

[2.5] Ratwani, M.M., *Analysis of Cracked Adhesively Bonded Laminated Structures*, American Institute of Aeronautics and Astronautics (AIAA), Volume 17, pp. 988-994, 1974.

[2.6] Ratwani, M.M., Kan, H.P., *Development of Composite Patches to Repair Complex Cracked Metallic Structures*, Volume I, Final Report NADC-80161-60, U.S. Navy, Naval Air Development Center, 1982.

[2.7] Duong, C.N., Yu, J., *The Stress Intensity Factor for a Cracked Stiffened Sheet Repaired with an Adhesively Bonded Composite Patch,* International Journal of Fracture, to be published.

[2.8] Hart-Smith, L.J., *Analysis and Design of Advanced Composite Bonded Joints,* NASA Langley Contract Report, NASA CR-2218, August 1974.

[2.9] Muki, R., Sternberg, E., *On the Stress Analysis of Overlapping Bonded Elastic Sheets*, International Journal of Solids and Structures, Volume 4, pp. 75-94, 1968.

[2.10] Rose, L.R.F., *An Application of the Inclusion Analogy,* International Journal of Solids and Structures, Volume 17, 1981, pp. 827-838.

[2.11] Rose, L.R.F., "Theoretical Analysis of Crack Patching" in: Baker, A.A., Jones, R., editors, *Bonded Repair of Aircraft Structures*, pp. 77-106, Martinus Nijhoff Publishers, Dordrecht, The Netherlands, 1988.

[2.12] Fredell, R.S., *Damage Tolerant Repair Techniques for Pressurized Aircraft Fuselages*, Wright Laboratory Technical Report 94-3134, June 1994.

[2.13] Rose, L.R.F., *A Cracked Plate Repaired by Bonded Reinforcements*, International Journal of Fracture, Volume 18, 1982, pp. 135-144.

[2.14] Lekhnitskii', S.G., *Anisotropic Plates*, Gordon and Breach Science Publishers, New York, 1968.

[2.15] Marissen, R., *Fatigue crack growth in ARALL; a hybrid aluminium-aramid composite material; crack growth mechanisms and quantitative predictions of the crack growth rates*, Phd Thesis, Delft University of Technology, Delft, 1988.

[2.16] Roebroeks, G.H.J.J., *Towards GLARE: The Development of a Fatigue Insensitive and Damage Tolerant Material*, Ph.D. thesis, Department of Aerospace Engineering, Delft University of Technology, Delft, the Netherlands, December 1991.

CHAPTER 3

PROCESSES AND MATERIALS FOR BONDED REPAIRS

3.1 Introduction to adhesively bonding

Even though adhesively bonding results in a greater structural efficiency, most (sub-) structural connections are still made with rivets. The fact that riveting is still the leading fastening method can be largely contributed to the long-lasting perception of poor service experience from the early years of bonded structures. However, due to examples as the Fokker F-27 (which has had over 30 years of outstanding service experience employing adhesively bonded metal primary structures) and the development of better adhesives, adhesion and pretreatment processes, adhesively bonding receives more and more attention. This section will give a short introduction into adhesively bonding. A more in-depth theoretical view can be found in [3.1], while the practical side of adhesively bonded repairs is well explained in [3.2].

The key feature of adhesively bonding is a uniform load transfer, contrary to mechanically fastening where load transfer is accomplished through discrete points. On top of that, bonding does not involve the removal of any load-bearing material, which is the case with riveting. Adhesively bonding can be summarized as the process of joining two or more materials, called adherends, by a continuous inter-layer of an adhesion-promoting substance, the adhesive.

In theory, the bonding process can be divided into two stages [3.1]. In the first stage, a good contact surface across the interface is made. The next stage is the generation of the adhesion forces across this interface. Throughout this stage a bond must be generated that is sufficiently strong and durable to ensure that the adhesive interface remains stronger that the adherends during service life. There are various kinds of adhesion forces, commonly referred to as mechanisms of adhesion. Several theories have been proposed (e.g. mechanical interlocking, diffusion theory, electronic theory and adsorption theory).

In order to achieve a good quality of the bondline, it is important to spread the adhesive evenly on the adherends. This can only be achieved when the adherends are free of contaminations such as oxides, paints, oil etc. The term describing the action of a liquid over the surface of an adherend is wettability. The key to a good wettability is a good surface pretreatment. This will be explained in the next paragraph.

3.2 Surface pretreatment

The most critical step in the adhesively bonding process is the preparation of the adherends to ensure good wettability, the so-called pretreatment [3.2]. In general, surface pretreatment processes contain the following steps [3.3]:

- degrease and rinse
- deoxidize and rinse
- chemically etch/anodize, rinse and dry
- prime

During the anodizing process, anodic coatings are "grown" on the bonding surface by passing an electric current through the adherend using a conductive acid medium. The adherend acts as the anode in an electrochemical cell, producing a stable oxide coating of typically 0.1 to 1.0 µm thick. The surface has a rough, interlocked appearance that can be described as "trees" and "antlers". Another method of roughening the surface is by grinding or grit blasting. These methods also remove old paint and oxide layers and increase the available area for bonding.

A primer is often applied after the etching/anodizing process. Adhesive primers are fundamentally adhesives that have been thinned down, using an organic solvent. A small amount of coupling agent is included in the primer. The primer has a dual function. Firstly, a primer is used to enhance the adhesion between the adhesive and the adherend. Secondly, due to the small amount of chromates and other corrosion inhibitors, corrosion within the bond line is prevented.

A widely accepted pretreatment in the aerospace industry is the PABST pretreatment. It involves degreasing of the adherends, deoxidizing in a chromic-sulfuric bath followed by phosphoric anodizing. The anodized surfaces are then air-dried, sprayed with an adhesion-promoting and corrosion-inhibiting primer and finally oven-cured. One of the main disadvantages of this method is the need for the adherends to be submerged in a tank. However, with the Boeing PACS (Phosphoric Acid Containment System), it is possible to perform phosphoric anodizing on the fuselage of an aircraft.

3.3 Inspection of bonded repairs

After the adherends are bonded, only non-destructive inspection methods can be used to inspect the bondline while keeping the bondline intact. For many years, the "coin tap"-method has been used by maintenance personnel for assessing bondline integrity. The success of this method is highly dependent on operator skill, experience and hearing acuity.

Several other methods can be used to check the bondline integrity [3.3]. The pulse-echo principle (sending sonic energy into the structure and measuring the reflection) has been used in the semi-automated, hand-portable "Woodpecker", which is used by many major airline maintenance departments. Another proven device is the Fokker Bond Tester, which uses a resonance-shift principle to detect debonds. More complex ultrasonic techniques, e.g. C-scan, are less suitable for in-field use because of the requirement of a couplant fluid. Through-transmission is virtually impossible for in-field use since unhindered access to both sides of the structure is required.

3.4 Materials used in crack patching

More and more, advanced composite materials are used in adhesively bonded repairs. Advanced composites can provide high structural efficiency to a repair and can be the only acceptable choice in certain cases. Crack patching is particularly attractive when replacement of the original cracked structure is exceptionally difficult or expensive. When applied according to state-of-the-art techniques, this results in a durable repair that will outperform riveted repairs.

The most commonly used materials and adhesives will be described here. It should be noted that the use of advanced materials and adhesives alone does not result in a good repair. As described in previous paragraphs, one of the most critical steps in the bonding process is the pretreatment of the adherends.

Composites
Repair materials that are already used by the Australian and United States Air Force are carbon- and boron-reinforced epoxy. Composites like these have a high modulus of elasticity, favorable for crack bridging, resulting in thin patches. Especially with thick repairs, secondary bending effects are becoming important.

However, the disadvantage of these materials is the large mismatch in coefficient of thermal expansion (CTE) between the repair material and the structure. Curing of the adhesive can result in considerable thermal tensile stresses on the crack flanks. The magnitude of this effect depends on the curing method. When using a heat blanket (as is commonly used with in-field repairs), the effect will be smaller than when curing in an autoclave because the expansion of the heated area is restricted by the surrounding cold structure, resulting in a lower effective CTE for the structure that is repaired. When curing in an autoclave, the complete assembly of structure and repair is heated, resulting in a larger mismatch in CTE and thus larger residual thermal stresses.

Besides these curing stresses, thermal stresses can occur while the aircraft is in service. At cruising altitude, the fuselage of an aircraft can cool down significantly, up to -54°C. The completely cooled structure of the aircraft will contract uniformly as if the material is unconstrained. In case of a low CTE patch (e.g. boron), the patch will not contract as much as the fuselage. The advantage of the constraint is not present anymore since the structure is not cooled locally. This will cause additional thermally induced stresses on the crack, combined with mechanical loading caused by the cabin pressure.
Tapering of the boron patches, in order to reduce stresses in the skin and adhesive at the patch tip, is accomplished by stepping down the length of the plies. The lay-up that is commonly used for composite patches is the inverted wedding cake lay-up, i.e. the largest ply is on the outside of the repair and the smallest ply is closest to the specimen. The advantage of the inverted wedding cake is that the number of free ply edges is reduced. Only the edge of the largest ply is exposed to the environment, the other plies are protected by this outer layer.

The properties of several materials involved in bonded repairs are given in table 3.1.

	2024-T3	**Ti 6Al-4V**	**GLARE2 3/2 0.2**	**boron/epoxy**	**carbon SP 500-2**
E_L (GPa)	72.4	116	69	207	186
E_{LT} (GPa)	72.4	116	54	19	12
α_L 10^{-6}/°C	22.5	7.1	16.3	4.5	-0.9
α_{LT} 10^{-6}/°C	22.5	7.1	24.5	20	26
$\sigma_{yield\ L}$ (MPa)	310	925	383	n/a	2913
$\sigma_{yield\ LT}$ (MPa)	310	925	242	n/a	n/a
$\sigma_{ultimate\ L}$ (MPa)	427	n/a	1187.5	1585	n/a
$\sigma_{ultimate\ LT}$ (MPa)	427	n/a	313.4	62.7	n/a

Table 3.1: Properties for some repair and parent structure material [3.4/3.5]

Fiber Metal Laminates
Fiber Metal Laminates are hybrid materials, consisting of thin aluminum and glass fiber/epoxy prepreg layers, and combines the characteristics of both materials. They will be treated here seperately because of their very specific characteristics.

GLARE® is a damage tolerant hybrid material developed at Delft University of Technology. It was originally developed for fatigue-critical aircraft structural applications [3.6]. GLARE® combines superior fatigue behavior and higher strength than monolithic aluminum, with a moderate stiffness. The CTE of GLARE® is higher than traditional composites such as boron-epoxy. As a patch material this results in a smaller difference in CTE with the parent (metal) structure (see table 3.1). Furthermore, it has good corrosion durability and impact behavior. Another advantage of FMLs is that the aluminum layers are primed and thus ready for bonding. Boron and carbon epoxy patches need to be grit-blasted before bonding.

FMLs consist of thin 0.2 to 0.5 mm aluminum alloy sheets, adhesively bonded in alternating layers with fiber/epoxy prepregs. Their excellent fatigue properties are due to the crack bridging effect of the fibers. A coding system is used to describe the lay-up of the laminate. For example, GLARE2-3/2-0.2 has a 3/2 lay-up, i.e. 3 layers of Al 2024-T3, each with a thickness of 0.2 mm,

separated by two unidirectional S2-glass fiber/epoxy prepreg layers (each with a thickness of 0.25 mm). An example of a 3/2 lay-up can be seen in figure 3.1.

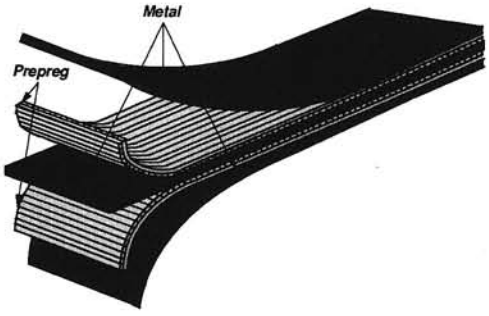

Figure 3.1: Typical fiber metal laminate 3/2 lay-up

Fiber Metal Laminates (FMLs) were initially developed to prevent rapid fatigue crack extension as it can occur in monolithic materials (see [3.7/3.8]). Even with large fatigue cracks present in the aluminum layers, a FML still shows an excellent fatigue performance thanks to fiber crack bridging. Crack bridging reduces the stress intensity at the crack tip considerably due to a considerable restraint on the crack tip opening by the bridging fibers. Therefore, the unbroken fibers in the cracked area still transmit part of the load through the crack.

Moreover, due to eccentricities present in the load path after crack patching, cracks will grow through the thickness. The stacked character of aluminum layers and fiber layers will prevent rapid crack growth through the thickness.

High strength of the repair is important for the damage tolerance characteristics of the repair. However, high stiffness is associated with increased load attraction. This load attraction will cause an increase in patch tip stresses as well as in crack tip stresses. GLARE® combines high strength with moderate stiffness.

Corrosion durability of the fiber metal laminates is excellent as well. The fiber layers in between the thin aluminum layers act as a barrier against through-the-thickness corrosion. Impact properties of fiber metal laminates are high. The aluminum layers allow plastic distortions and the fiber layers absorb large amounts of kinetic energy. Repaired impact sensitive locations have limited loss of strength after second impact.

3.5 Choice of the adhesive

Before selecting a repair adhesive, it is important to know what the exact application of the adhesive will be. The choice should be based on the required strength and durability, type of available equipment to apply the repair and, one of the most important points, the expected service temperature range [3.9].

The adhesives available for structural bonding can be categorized in three groups:
- Film adhesives
- Past adhesives
- Foam adhesives

Film adhesives are the type that is most used in the field of bonded repairs. Film adhesives are made by blending high molecular weight polymers with curing agents, fillers and other compounding ingredients, then formed into thin films.

Film adhesives have several very important advantages over the other two adhesives:
- They do not require mixing prior to use.
- They are easy to handle.
- They have better uniform bondline thickness with a carrier cloth.
- They have a more uniform composition.

Film adhesives have some disadvantages:
- They require pressure and heat to cure the adhesive.
- They have a short shelf life.
- They require cold storage, which can be a problem for field repairs (although 24 hours without refrigeration is no problem in most cases).
- They are more expensive than paste adhesives.

In selecting an adhesive for a structural repair, the first disadvantage is of major interest. There are several reasons why high cure temperatures should be avoided [3.10]:
- It is difficult to achieve and control locally elevated temperatures in a complicated structure under field conditions.
- It is possible that unwanted metallurgical changes will take place in the parent structure.
- Development of detrimental thermal residual stresses in the structure (see paragraph 4.2).

It is hard to avoid the use of adhesives that require elevated cure temperatures. Room temperature adhesives can be useful for some applications, but the structural film adhesives, cured at elevated temperatures, provide the best properties for structural applications over a wide temperature range.

[3.1] Kinloch, A.J., *Adhesion and Adhesives - Science and Technology*, Chapman and Hall, London, 1987

[3.2] Reinhart, T.J., "Surface treatments for bonded repairs of metallic components" in: Baker, A.A., Jones, R., editors, *Bonded Repair of Aircraft Structures*, pp. 19-30, Martinus Nijhoff Publishers, Dordrecht, The Netherlands, 1988.

[3.3] Fredell, R.S., *Damage Tolerant Repair Techniques for Pressurized Aircraft Fuselages*, Wright Laboratory Technical Report 94-3134, June 1994.

[3.4] Fredell, R.S., Department of Engineering Mechanics, U.S. Air Force Academy, Colorado, Van Barneveld, W., Vlot, A., Faculty of Aerospace Engineering, Delft University of Technology, The Netherlands, *Analysis of Composite Crack Patching of Fuselage Structures: High Patch Elastic Modulus isn't the Whole Story*, 39th International SAMPE Symposium, Anaheim, California, April 11-14 1994.

[3.5] *CalcuRep® for Windows*, version 1.0, February 6 1997.

[3.6] Vogelesang, J.B., Schijve, J., Fredell, R.S., *Fibre-metal laminates: damage tolerant aerospace materials*, Case Studies in Manufacturing with Advanced Materials, Volume 2, 1995.

[3.7] Marissen, R., *Fatigue crack growth in ARALL; a hybrid aluminium-aramid composite material; crack growth mechanisms and quantitative predictions of the crack growth rates*, Ph.D. thesis, Delft University of Technology, Delft, 1988.

[3.8] Roebroeks, G.H.J.J., *Towards GLARE: The Development of a Fatigue Insensitive and Damage Tolerant Material*, Ph.D. thesis, Department of Aerospace Engineering, Delft University of Technology, Delft, the Netherlands, December 1991.

[3.9] Kelly, L.J., "Introductory chapter" in: Baker, A.A., Jones, R., editors, *Bonded Repair of Aircraft Structures*, pp. 1-18, Martinus Nijhoff Publishers, Dordrecht, The Netherlands, 1988.

[3.10] Baker, A.A., "Crack Patching: experimental studies, practical applications" in: Baker, A.A., Jones, R., editors, *Bonded Repair of Aircraft Structures*, pp. 107-173, Martinus Nijhoff Publishers, Dordrecht, The Netherlands, 1988.

CHAPTER 4

CALCUREP® AND THE EXTENSIONS TO THE ROSE MODEL

4.1 Introduction to CalcuRep®

Before airlines and airworthiness authorities will consider crack patching a viable repair alternative, it is important that the analysis, as described in chapter 2, can be performed in the field by an aircraft maintenance engineer. This implies that the complex analysis must be transformed to a user-friendly and easy-to-use software package for design and analysis with conservative engineering guidelines so that acceptable repairs can be designed. Until recently, the detailed design and (analytical) analysis of bonded repairs could only be performed by specialist teams, due to the complexity of the analysis.

In close cooperation, Delft University of Technology and the United States Air Force Academy have developed a software package, CalcuRep®, that allows non-specialists, such as maintenance engineers with limited knowledge of bonded repair analysis, to design and analyze bonded repairs. CalcuRep® contains pull-down menus of material, mechanical and physical properties that are easy to use, and the output consists of acceptability guidelines.

The analytical model in CalcuRep® is based on the Rose model as presented in chapter 2. As is explained in that chapter, the Rose model is a continuum two-dimensional model that considers only elliptical patches, bonded to infinite flat sheets under bi-axial loading. In CalcuRep®, the Rose model has been extended to include the important thermal effects, induced by curing of the adhesive and by operating temperatures. The second extension that has been added calculates the effect of bending induced by a single-sided repair. These two extensions will be discussed in detail in paragraph 4.2 and 4.3.

With CalcuRep® it is possible to quickly optimize the patch material and geometry with respect to the stress intensity reduction at the crack tip and the adhesive shear strain, for a given fuselage, adhesive system and cruise temperature.

CalcuRep® calculates the following important design parameters [4.1]:

- the repaired stress intensity factor K at the crack tip,
- the maximum stress in the patch (over the crack),
- the maximum skin stress (at the patch tips),
- the maximum shear strain in the adhesive,
- the shear load transfer length in the bond line.

With these parameters, the critical locations (figure 4.1) in a bonded repair can be evaluated.

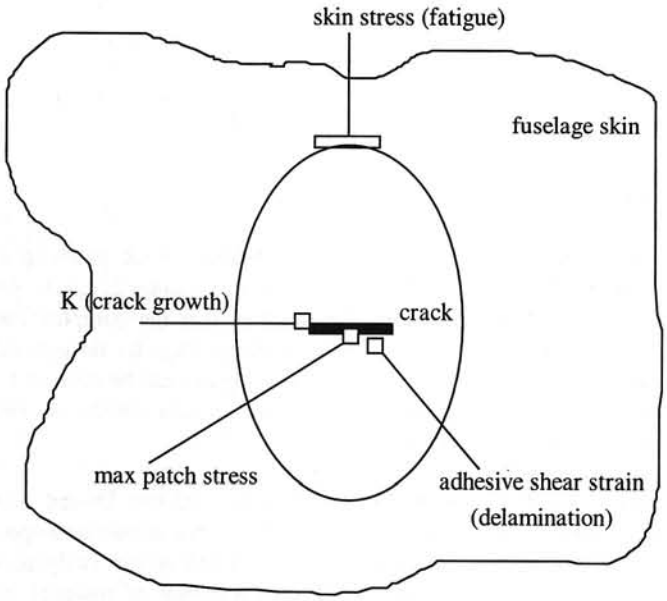

Figure 4.1: Possible failure modes in an adhesively bonded repair

Each location refers to a particular failure mode in the bonded repair. They can be summarized as follows:

- crack growth of the repaired crack due to a too high repaired stress intensity factor at the crack tip, which influences inspection intervals,
- shear failure of the adhesive,
- creep failure and debonding of the bond line due to sustained shear loading,
- debonds due to peel stresses at the patch tip,
- re-initiation of new fatigue cracks at the patch tips,
- fatigue failure of the patch itself.

With the CalcuRep® output and design help screen, it is possible to quickly change the repair design iteratively toward a satisfactory and safe repair.

4.2 Thermal stresses

Repaired structures are usually subjected to two types of loading: mechanical and thermal loading. The next two sections will describe the theoretical background of thermal residual stresses [4.2]. The third section will describe the analytical model that is used in CalcuRep® to calculate the magnitude of the thermal residual stresses.

4.2.1 Thermal residual stresses in an unsupported structure

Different materials are involved when applying a bonded repair. Not only different repair materials; the parent structures can be made of different materials too. Each of these materials and, more importantly, the combination of materials, have their own advantages and disadvantages. The properties of several materials were given in table 3.1. Two repair materials, boron-epoxy and GLARE®, will be compared in this section.

Boron repair
As can be seen, the coefficient of thermal expansion (CTE) in the longitudinal direction of boron ($4.5x10^{-6}$/°C) is low compared to the CTE of the aluminum 2024-T3 ($22.5x10^{-6}$/°C). During the cure cycle in the unconstrained situation, as is the case when applying a patch to a test specimen, both materials are able to expand freely. The uncured adhesive is no restriction for both materials to expand. After curing at elevated temperatures, the adhesive will change into the cured state and bond the two materials.

When the temperature falls after curing, the aluminum will contract more than the boron and, since the adhesive is set, the parts cannot contract unrestricted and the boron patch will put tensile stresses on the repaired crack in the panel. The panel will show a curvature, which is a good indication for thermal residual stresses.

GLARE® repair
GLARE2 has a thermal coefficient of expansion of $16.3x10^{-6}$/°C, which is still lower than the CTE of Al 2024-T3. This means that by cooling down from 120°C, the aluminum still contracts more than the GLARE® patch. This will again cause residual thermal tensile stresses on the crack, although lower than in the case of the boron patch. This can be noticed when comparing panels patched with boron and with GLARE®, the curvature in the panel with the GLARE® patch is noticeably smaller than in the panel with the boron patch.

If these panels, which are repaired in an unconstrained condition, are cooled down to cruise altitude temperatures, the aluminum will still contract more than the patches, resulting in additional tensile thermal stresses on the crack faces. Repairs made in an unconstrained situation tested at the lowest service temperature represent the worst case scenario with regards to thermal stresses and will result in conservative test results.

4.2.2 Thermal residual stresses in a stiffened structure

The situation for a stiffened aluminum structure, as it is seen in an actual airplane, is different. The restraint, due to the stiffening of the structure, can be highly beneficial in lowering the thermal residual stresses in the repaired section by reducing the coefficient of thermal expansion in the heated zone. The level of restraint depends largely on the stiffness and (lower) temperature of the surrounding structure. In a typical aircraft structure, the restraint is relatively high due to the size of the structure, the rigid fastening of the components [4.3], and the surrounding cold structure.

The coefficient of thermal expansion of the repaired constrained structure will be significantly lower than that of unconstrained small aluminum sheet material, as is used in test specimens. Experiments and analytical studies show the influence of different constraints on the thermal stresses in the repaired structure. More about this can be found in [4.4/4.5/4.6].

Boron repair
When considering a repair of a constrained cracked structure with a boron patch, the difference in CTE will be significantly lower than in the case of the unconstrained structure. After cooling to room temperature, the bond line for patch materials with relatively low coefficients of thermal expansion (CTE), like boron- or carbon-fiber composites, is relatively stress free. In other words, the stress intensity range, ΔK, will be smaller than for the unconstrained case resulting in lower crack growth rates. The adhesive shear strains in the adhesive will also be smaller.

GLARE® repair
When considering a repair of a constrained cracked structure with a GLARE® patch, an additional beneficial effect can take place. The difference in CTE is not very large and, if the CTE of the structure is lower because of the constraint, the effective CTE can become lower than the CTE of the GLARE® patch. This is where GLARE® becomes very interesting as a repair material for thin-skinned structures. Since the effective CTE of the structure is lower than the CTE of the patch, the patch will contract more than the heated area when cooling down to room temperature, resulting in residual thermal compressive stresses on the crack. Whereas boron results in an almost stress free situation for the constrained case, GLARE® patches actually close the crack, resulting in smaller crack opening displacements and thus a lower stress intensity factor range ΔK. This will result in lower crack growth rates of the repaired crack. Figure 4.2 shows the repaired situations for low and high CTE patch materials.

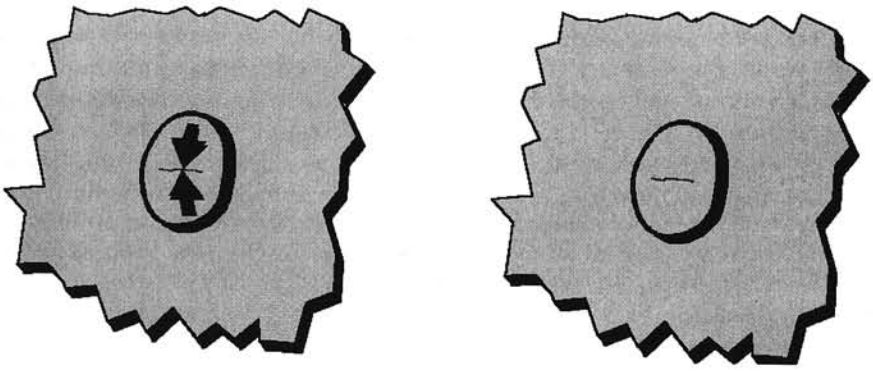

High CTE patch (GLARE®) *Low CTE patch (boron-epoxy)*

Figure 4.2: Thermal effects in skin at room temperature [4.7]

In some operational conditions, the fuselage of an aircraft can cool down significantly, up to -54°C. The now completely cooled structure of the aircraft will contract uniformly as if the material is unconstrained. In case of a low CTE patch, the patch will not contract as much as the fuselage. The advantage of the constraint is not present anymore since the structure is not cooled locally. This will cause additional thermally induced stresses on the crack combined with mechanical loading by the cabin pressure. An additional problem might be that the adhesive becomes more brittle compared to the situation at room temperature.

A high CTE patch will still put some beneficial compressive stresses in the skin at cruise altitude. Figure 4.3 shows the repaired situation for low and high CTE patches at cruise altitude.

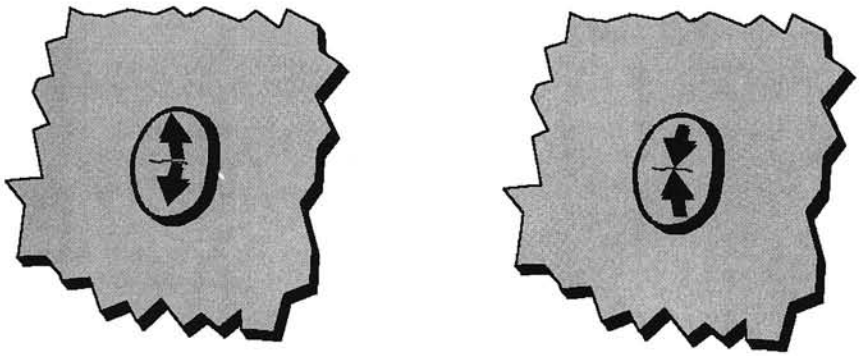

Low CTE patch (boron-epoxy) *High CTE patch (GLARE®)*

Figure 4.3: Thermal effects in skin at cruise altitude [4.7]

4.2.3 Thermal stress calculations

The thermal expansion analysis is quite complex. A simple multiplication of the difference in CTE between the patch and plate, by the difference between the curing and room temperature, overestimates the thermal stress problem [4.8]. For the repairs of thick sections (like fighter aircraft wing structures), the residual thermal stresses are less severe [4.9] since the surrounding (unheated) structure limits free expansion of the heated area. This results in lower thermal residual stresses after cooling. In the repair of a relatively thin fuselage structure, the constraint is smaller. Furthermore, the skin may deform locally out of plane during heating. This section describes how CalcuRep® calculates the effective CTE of the structure and the thermal stresses that arise due to a mismatch in CTE.

The thermal analysis incorporated in CalcuRep® is done for both the curing stresses as well as for thermal stresses due to the usage of the aircraft. A constant pre-load will exist after curing when there is a mismatch between the CTE of the patch and the skin. For equilibrium the stresses underneath the patch will be balanced by stresses at the patch boundary. These stresses result in residual membrane stresses at the patch edge, increasing the average stress [4.10].

The equations, governing the thermal behavior, are derived using LaPlace's potential equation [4.8]. The analysis considers a steady-state temperature field in a circular isotropic plate of radius R as represented by figure 4.4. The plate is heated to a temperature T_c over a central circular region of radius d by means of a thermostatically controlled heat blanket. Furthermore, the thermal conductivity of the plate is assumed to be independent of the temperature T.

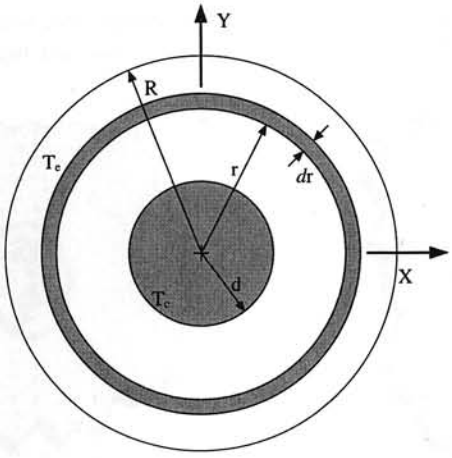

Figure 4.4: Model for calculation of temperature in a circular isotropic patch.

Thus:

$$\nabla^2 T = 0 \qquad (4.1)$$

With the assumption of constant through-the-thickness temperature in the skin equation 4.1 can be written as:

$$\frac{d^2T}{dr^2}+\frac{1}{r}\frac{dT}{dr}=0 \qquad (4.2)$$

with boundary conditions:

$T = T_c$ at $r = d$,
$T = T_e$ at $r = R$.

The solution of equation 4.2 is given as:

$$T = T_e + \frac{(T_c + T_e)\ln\left(\frac{r}{R}\right)}{\ln\left(\frac{d}{R}\right)}, \qquad R \geq r \geq d. \qquad (4.3)$$

$$T = T_c, \qquad r \leq d.$$

The heat transfer rate $\dot{Q}$ which crosses the outer surface area A of the solid ring with width dr is given by:

$$\dot{Q} = hA(r)[T(r) - T_\infty] \qquad (4.4)$$

where h = the coefficient of heat transfer,
$A(r)$ = the strip surface area at radius r,
$T(r)$ = the temperature of the plate at radius r,
T_∞ = the temperature of the cooling medium (air).

Now, the final expression of T_e is given as (the full derivation can be found in appendix C of [4.8]):

$$T_e = (T_c - T_{ambient})e^{-m(R-d)} + T_{ambient} \qquad (4.5)$$

where m is a heat transfer constant defined in appendix C of [4.8].

The expressions as defined above, are used to determine the effective coefficient of thermal expansion which is used to determine the thermal stresses.

During the cure cycle, the effective CTE of the plate is smaller due to free expansion restriction by the cold surrounding structure. The effective coefficient of thermal expansion (α_{Peff}) is given as:

$$\alpha_{Peff} = \frac{\alpha_P}{2}(1+\nu_P)\left\{1-\frac{T_e}{T_c}+\frac{d^2}{R^2}\left(\frac{T_e}{T_c}-1\right)-\frac{1-\frac{T_e}{T_c}}{2\ln\left(\frac{d}{r}\right)}\left[\frac{d^2}{R^2}-1-\frac{2d^2}{R^2}\ln\left(\frac{d}{R}\right)\right]\right\} \qquad (4.6)$$

During the flight at cruise altitude, the surrounding structure provides no constraint, making the expression for the effective CTE less complex:

$$\alpha_{Peff} = \alpha_P \qquad (4.7)$$

Finally, the residual thermal stresses can be calculated with the analysis for a two-dimensional statically undetermined structure. The problem involves three distinct elements:

- the reinforced region of the plate (the skin under the patch),
- the reinforcement (the patch),
- the surrounding matrix.

The extensive calculation can be found in appendix C of [4.8].

Some comparison has been made between boron and GLARE® with and without thermal effects taken into account [4.7]. The comparison was made for the case of a Boeing 737-200 fuselage at a cruising altitude of 10000 m. The 2024-T3 skin is 1 mm thick, the crack length is 51 mm. The patch length is 140 mm, and the patch width is 102 mm, for both materials the same. To bond the patches to the panel, AF-163-2K (3M) was used, the shear modulus G and the yield strength τ_{yield}, were corrected for the cruising altitude. The results of this comparison can be seen in figure 4.5.

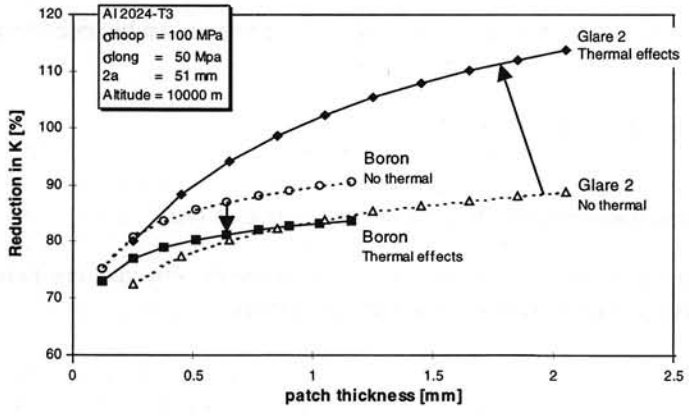

Figure 4.5: Comparison of reduction in stress intensity factor for bonded GLARE2 and boron patches, with and without considering thermal effects [4.7]

As can be seen from figure 4.5, if no thermal effects are taken into account, the stiffer boron/epoxy outperforms the GLARE®. However, when the thermal effects due to bonding and due to cruise at high altitudes are taken into account, GLARE® easily outperforms the boron/epoxy. As expected, the performance of the boron/epoxy is diminished as the additional residual thermal tensile stresses on the crack are taken into account.

4.2.4 Measurements of residual thermal stresses on a F-28 fuselage

In order to verify the magnitude of residual thermal stresses, a section of a Fokker F-28 fuselage was instrumented with strain gauges and thermocouples, and tested in the laboratory [4.11]. The section is situated between the wing and cockpit and has a length of 3.0 m and a diameter of 3.5 m. The skin is made out of Al 2024-T3 clad with a thickness of 1.0 mm. The frame distance is 500 mm and the stiffener pitch is 170 mm. The internal strains, which are present during and after curing, were determined. Also the out-of-plane deflection of the skin during curing was recorded.

The GLARE® patches were bonded to the outside of the fuselage with AF-163-2K (3M), which cures at elevated temperatures. It has a thickness of 0.13 mm. Patches were bonded to three different locations:

- Patch 1 on uncracked skin in the center between two stringers and frames.
- Patch 2 on same location but with a crack (saw cut) in the skin.
- Patch 3 over a riveted/bonded lap joint, no crack.

Repairs 1 and 2 are the most unfavorable locations with respect to possible out of plane deformation. Repair 3 is located on a position known for fatigue damage. More information about the repairs can be seen in table 4.1.

Repair no.	Patch material	Patch size (mm)	Curing process
1	GLARE3 3/2 0.2	175 x 110	5 hrs. at 90°C 1 hr. at 120°C
2	GLARE2 3/2 0.2	205 x 140	5 hrs. at 95°C
3	GLARE2 3/2 0.2	205 x 140	5 hrs. at 95°C

Table 4.1: Material, patch and cure information

The following observations were made:

- Repair 1: Significant out of plane bending of the skin towards the outside of the fuselage occurred during curing at 90°C, accompanied by torsion of the adjacent stringers. At 90°C, 3.4 mm displacement of the skin and a stringer displacement sidewards of 3.0 mm were measured. After cooling down to room temperature, 0.73 mm of the skin deflection appeared to be permanent.
- Repair 2: At 95°C, 4.0 mm displacement of the skin at the center of the repair was observed, 1.14 mm was permanent.
- Repair 3: Due to the location of this repair, the deflection was smaller than for repair 1 and 2. A deflection of 2.64 mm was measured at 95°C of which only 0.14 mm was permanent.

An initial cure of the adhesive at lower temperatures followed by a post-cure at the required cure temperature is recommended. Especially a repair location with a thin skin without a stringer or frame underneath should be treated carefully. Residual out-of-plane deflection, even the small deflection for repair 3, will certainly have an influence on the residual stresses.

A comparison of the temperature distributions in both circumferential and longitudinal direction revealed that the temperature prediction by the Rose model somewhat overestimates the measured distribution (max. 20%, see figure 4.6). The temperature drop is faster in circumferential direction than in longitudinal direction. This is due to the heat transfer in the stringers. There are three possible explanations for the overestimation of Rose's model. The model only takes into account the heat transfer in the plane of the skin. In reality, heat will also be transferred to the surrounding air, which will cause a lower temperature than predicted. Also the heat transfer by the stringers and frames is not accounted for in the model. A third explanation can be the fact that the temperature under the heat blanket is assumed to be constant which is not the case in reality. Nevertheless, the correspondence between the model and reality is satisfactory.

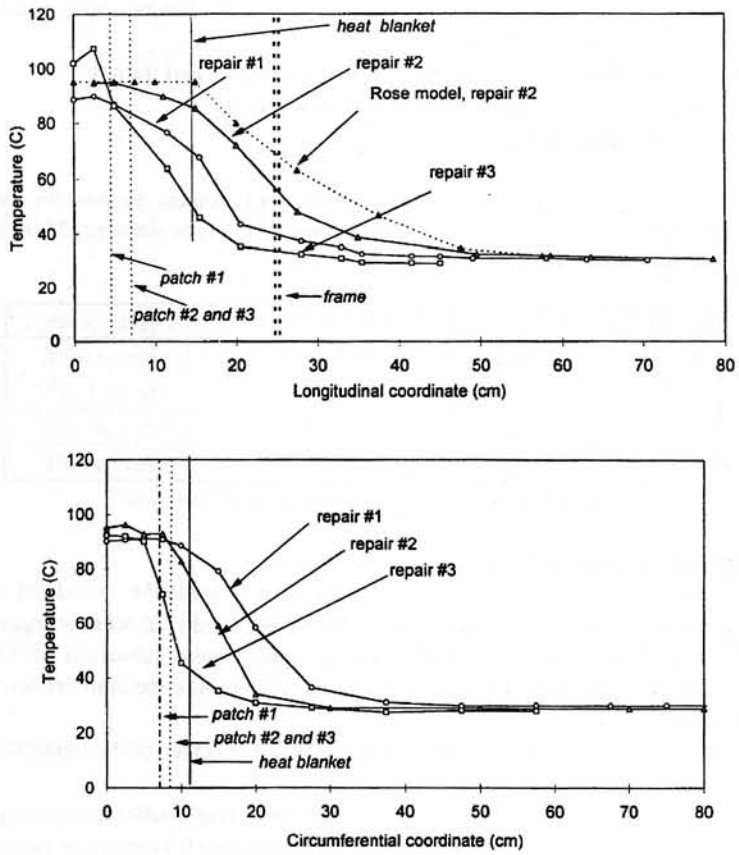

Figure 4.6: Measured temperature distributions [4.11]

4.3 Neutral Line Model for bending calculations

4.3.1 Introduction to secondary bending

One of the assumptions made in the Rose model is the restriction of out-of-plane bending of the repaired structure (see paragraph 2.2). Fredell states [4.8]: "(The Rose model) ignores that a single-sided patch will induce some bending from eccentricity. However, as the likely repair situation in a fuselage will be on or near stiffening elements, out-of-plane displacement will be restrained. Thus, secondary bending effects should be absent".

However, in most cases this stiffener is not attached to the critical top row of rivets, but to the middle or lower row. Next to that, bending restraint of a stiffener is much higher in the longitudinal direction (parallel to crack growth direction) than it is in circumferential direction. This way, a certain amount of out-of-plane deflection of the crack surfaces is allowed, as can be seen in figure 4.7.

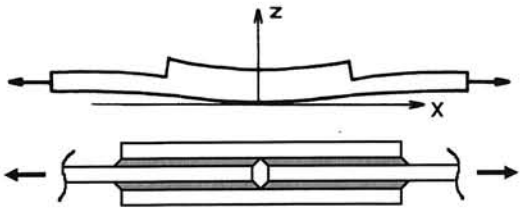

Figure 4.7: Single-sided and double-sided repair

Secondary bending can determine as much as 50% of the stresses at critical locations such as patch tips and splice plates. At crack faces, secondary bending can also be significant, especially with larger cracks and thicker adherends. It can stimulate crack growth and the formation of debonds. So far, CalcuRep® does not account for secondary bending at crack flanks.

Secondary bending in single-sided repairs is related to three important phenomena:

- applied stress and load attraction,
- geometry of the patch,
- geometry of the repaired structure.

The applied stress and the eccentricity determine the bending moment at the patch tip. This bending moment, the extensional stiffness and the flexural rigidity of adherend and patch determine the bending stresses. However, due to the 3D-character of the repaired structure, load attraction will occur due to the larger stiffness of the repaired area. This additional load contributes to the applied load and causes local stress increases at the patch tip in the skin.

4.3.2 The Neutral Line Model

In CalcuRep® the additional secondary bending stresses in the plate at the patch tip are calculated with the two-dimensional Neutral Line Model (NLM). With the NLM, good indications can be given for stresses at the critical patch locations. A bending moment is introduced in the structure due to a shift in the neutral line of the structure at the boundaries of the patch, caused by the eccentricity of the repair. The NLM calculates the stress system in a non-linear way, which is rather essential in case of secondary bending since secondary bending stresses will be largely overestimated with a linear approach.

The main withdrawal of a two-dimensional model is that it will overestimate the magnitude of the bending stresses at the crack tip since load shedding around the crack is ignored. Despite the model being two-dimensional, good indications can be obtained for the patch design. An even better quantification of bending stresses at the crack tip in the patch can be determined with empirical correction factors.

Assuming:

- plane stress in the x-z plane,
- plane strain in the x-y plane,
- plates are isotropic and of constant thickness,
- adherends are analyzed as flat plates under bending,

the bending moment can be derived as follows (see figure 4.8 for sign convention).

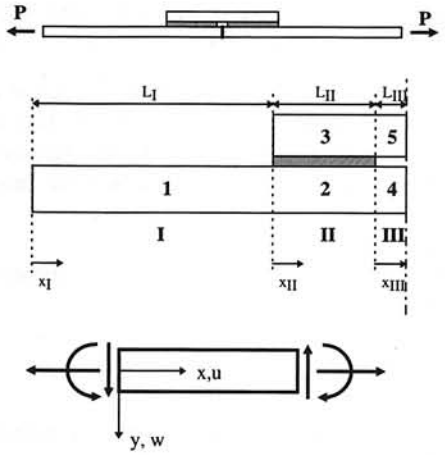

Figure 4.8: Patched skin repair under general loading

The NLM is a model of an infinitely wide plate with an integral infinitely wide strip of length $2a$. A second order differential equation is used to correlate the deflection during loading to the bending stress. The deflection of the neutral line due to an applied load P can be described by the following differential equation:

$$M_x = Pw = E_i I_i \frac{d^2w}{dx^2} \Rightarrow \frac{d^2w}{dx^2} - \alpha_i^2 w = 0 \qquad (4.8)$$

where

$$\alpha_i^2 = \frac{P}{E_i I_i} \tag{4.9}$$

and where x is the coordinate along the line of action of the applied load, w is the separation between the neutral line and the line of action and i denotes each part of the model with a specific flexural rigidity.

The solution of the differential equation is:

$$w_i = A_i \cdot sinh(\alpha_i x) + B_i \cdot cosh(\alpha_i x) \tag{4.10}$$

The bending stress is obtained from the flexure formula:

$$\sigma_{bending} = \frac{M_x z}{I} = \frac{P \cdot w(x) \cdot z}{I} \tag{4.11}$$

where z is the coordinate perpendicular to the neutral line in the modeled cross-section. The secondary bending is influenced by the load attraction effect. This is most pronounced at the patch tips and is taken into account by taking for P the tip stress multiplied by the skin thickness. More about this can be found in 4.3.3.

When e_{s_p} and e_{2_p} denote the jump of the neutral line at the transition between respectively section I and II, and section II and III, the following boundary conditions can be derived using compatibility conditions:

$$\begin{aligned}
&w_I\big|_{x_I=0} = 0 \\
&w_{II}\big|_{x_{II}=0} = w_I\big|_{x_I=L_I} - e_{s_p} \\
&\left.\frac{dw_{II}}{dx}\right|_{x_{II}=0} = \left.\frac{dw_I}{dx}\right|_{x_I=L_I} \\
&w_{III}\big|_{x_{III}=0} = w_{II}\big|_{x_{II}=L_{II}} - e_{2_p} \\
&\left.\frac{dw_{III}}{dx}\right|_{x_{III}=0} = \left.\frac{dw_{II}}{dx}\right|_{x_{II}=L_{II}} \\
&\left.\frac{dw_{III}}{dx}\right|_{x_{III}=L_{III}} = 0
\end{aligned} \tag{4.12}$$

These six boundary conditions can be used to determine the six unknowns A_I - A_{III} and B_I - B_{III}. Now the moment at $x_{II} = 0$ and $x_{III} = 0$ can be calculated with equation 4.8. When no debond is present, the deflection of the neutral line can be seen in figure 4.9.

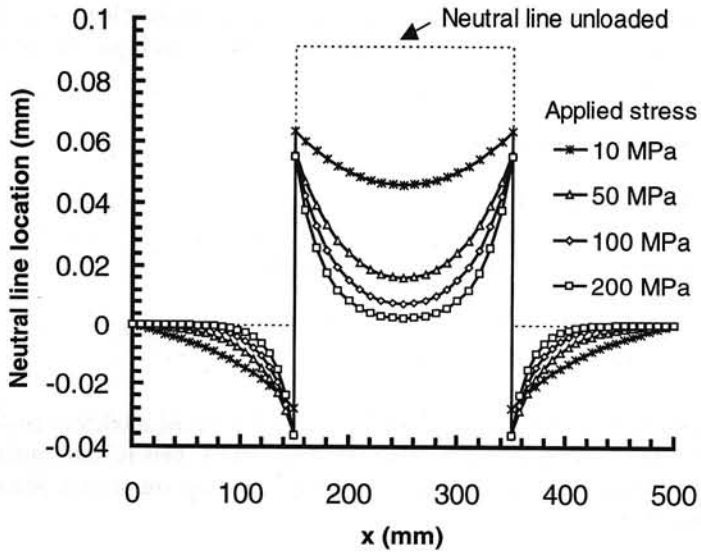

Figure 4.9: Deformation of the neutral axis of a single sided patch repair as function of applied load (GLARE 2 3/2 0.2 patch, length 200 mm on a 1 mm thick Al 2024-T3 skin)

With this model several improvements can be made to the Rose model. The Neutral Line Model results in good stress predictions but remains a two-dimensional estimation. Also, the laminated character of GLARE® is not accounted for. Taking the average flexural rigidity and consecutively calculate the stress in the layer with the highest secondary bending will result in a small error.

4.4 Conclusions

From this chapter, it can be concluded that CalcuRep® is a useful and easy to use design tool for bonded repairs. Two important extensions to the Rose model have been succesfully implemented, thermal stress calculations and secondary bending. Currently, extensions are being made to CalcuRep® in order to be able to design repairs for more complex structures in the vicinity of e.g. frames and stringers.

[4.1] Vlot, A., Fredell, R.S., Guijt, C.B., Ipenburg, G., Müller, R.P.G., *Bonded Fiber Metal Laminates Repair Patches For Aircraft Fuselages*, Proc. 10th Int'l. Symp. Swiss Bonding, pp. 265-280, Switzerland, May 1996.

[4.2] Verhoeven, S., *In-Service Effects on Crack Growth under Bonded Composite Repairs*, Master Thesis, Delft University of Technology, The Netherlands, July 21st, 1998.

[4.3] Baker, A.A., "Crack Patching: experimental studies, practical applications" in : Baker, A.A., Jones, R., editors, *Bonded Repair of Aircraft Structures*, pp. 107-173, Martinus Nijhoff Publishers, Dordrecht, The Netherlands, 1988.

[4.4] Baker, A.A., Davis, M.J., Hawkes, G.A., *Proceedings on the 10th International Committee on Aeronautical Fatigue (ICAF) Symposium*, paper 4.3, 1979.

[4.5] Rose, L.R.F., *International Journal of Fracture 18*, pp. 135-144, 1982.

[4.6] Jones, R., Callinan, R.J., *Journal of Structural Mechanics 8*, (2), pp. 143-149, 1980.

[4.7] Fredell, R.S., USAF, Department of Engineering Mechanics, U.S. Air Force Academy, Colorado, Schelling, J.A., Faculty of Aerospace Engineering, Delft University of Technology, The Netherlands, *Thermal Effects in Bonded Repairs to Cracked Fuselages*, to be published.

[4.8] Fredell, R.S., *Damage Tolerant Repair Techniques for Pressurized Aircraft Fuselages*, Wright Laboratory Technical Report 94-3134, June 1994.

[4.9] Rose, L.R.F., "Theoretical Analysis of Crack Patching" in: Baker, A.A., Jones, R., editors, *Bonded Repair of Aircraft Structures*, pp. 77-106, Martinus Nijhoff Publishers, Dordrecht, The Netherlands, 1988.

[4.10] Fredell, R.S., Van Barneveld, W., Vlot, A., *Analysis of Composite Crack Patching of Fuselage Structures: High Patch Elastic Modulus Isn't the Whole Story*, Proc. 39th international SAMPE symposium, Anaheim, pp. 610-623, 1994.

[4.11] Vlot, A., Soerjanto, T., Yeri, I., and Schelling, J.A., *Residual Thermal Stresses Around Bonded Fibre Metal Laminate Repair Patches on an Aircraft Fuselage*, Proceedings 41st International SAMPE Symposium, Anaheim, California, 1996.

CHAPTER 5

ANALYSES OF STRESS INTENSITY FACTORS AND STRESSES IN THE PERIPHERY OF BONDED REPAIRS, USING FEM AND NLM

As was mentioned before, CalcuRep® is based on an analytical model in order to enable maintenance personnel to easily design and analyze bonded repairs. At this moment, only single repairs with a limited geometrical complexity are implemented in CalcuRep®, making it necessary to develop other methods that allow the analyses of more complex situations. Therefore, FEM calculations are being performed, using the latest FEM programs. Although FEM calculations are suitable to analyze more complex repairs, they are more complicated to implement and require specialists. Several problems were analyzed and the results will be given in this chapter. Also some calculations were done by making extensions to the Neutral Line Model (NLM).

5.1 Stresses in the periphery of bonded repairs

5.1.1 The influence of patch separation on load attraction

One of the topics that was recently investigated using FE modeling, is the interaction effect of multiple patches in close proximity of each other [5.1]. It would be convenient to be able to use an analytical model for the prediction of this influence but the Rose model can only analyze single patches, it is complex to use Lekhnitskii's inclusion theory [5.2] for multiple patches.

To investigate the load attraction effects in the case of multiple patches, a linear 2D FE-program was used, which incorporated a 12-node bi-cubic shell element. Only uni-axial loads and stresses in loading direction were considered. A realistic crack was not included in the model. The influence of the crack on the stresses in the skin around a patch was considered to be small.

Using this FE-program, two different configurations were considered (figure 5.1):

- a row of patches perpendicular to the applied load
- a row of patches parallel to the applied load, also called a "column of patches"

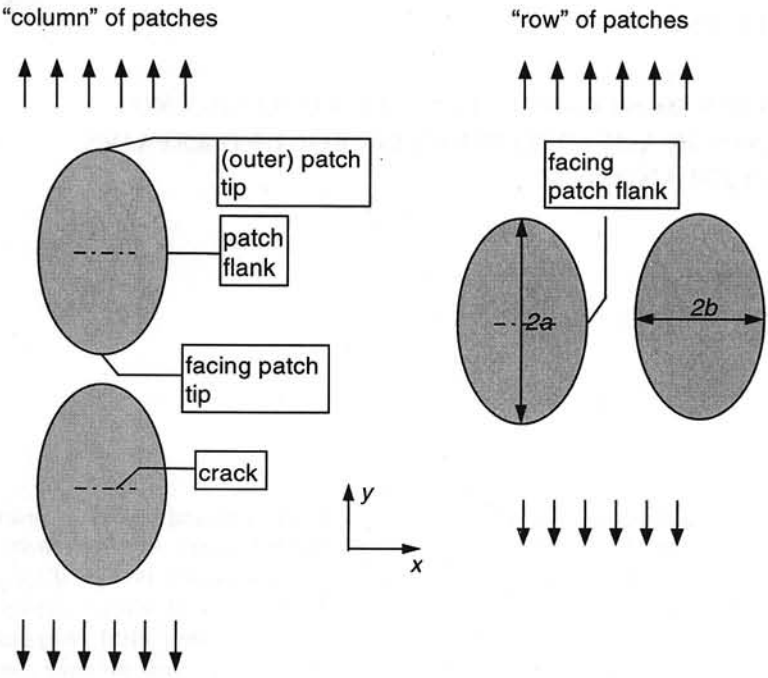

Figure 5.1: Orientation of multiple patches [5.1]

Row of patches

First a row of two patches is considered, perpendicular to the applied load. A row of two patches can be necessary for a MSD repair; multiple fuselage patches along a longitudinal lap joint. In case of a finite row of two patches, only half a patch needs to be modeled and one specimen edge remains free of loads and boundary conditions.

Both a circular and an elliptical (aspect ratio a/b of 0.5) patch have been examined with the 2D linear finite element analysis. The patch separation is expressed as the ratio of the absolute separation, S_p, and the patch width b,: S_p/b.

The results of the circular patches are plotted in figure 5.2. From this analysis, it is clear that load attraction as an interaction effect is determined by the ratio of absolute separation relative to patch width, S_p/b. Figure 5.2 shows that the stress at the outer flanks of a finite row is consistently 36% lower than the applied stress. Obviously, the stress at the outer flanks is not influenced by the patch separation when the separation is more than 0.1b. From the same figure it can be concluded that the stresses at the tips and the inside flanks decrease slightly with decreasing separation.

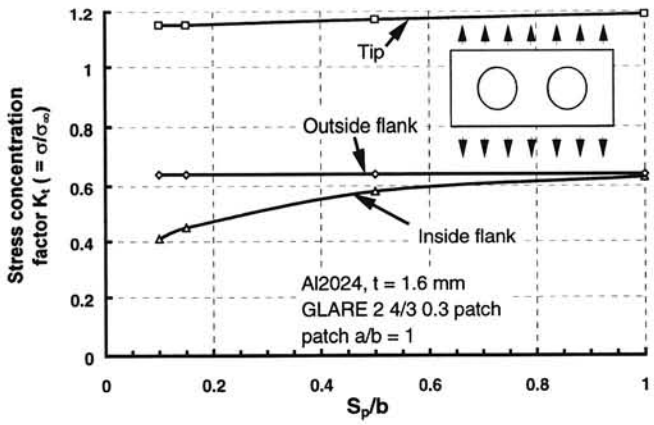

Figure 5.2: Stress concentration factors in a row of two circular patches (a is half patch length, b is half patch width) [5.1]

When two elliptical patches (a/b = 0.5) are used, skin stresses at the outside flanks show a slight increase with decreasing patch spacing. However, the change in magnitude remains marginal (figure 5.3).

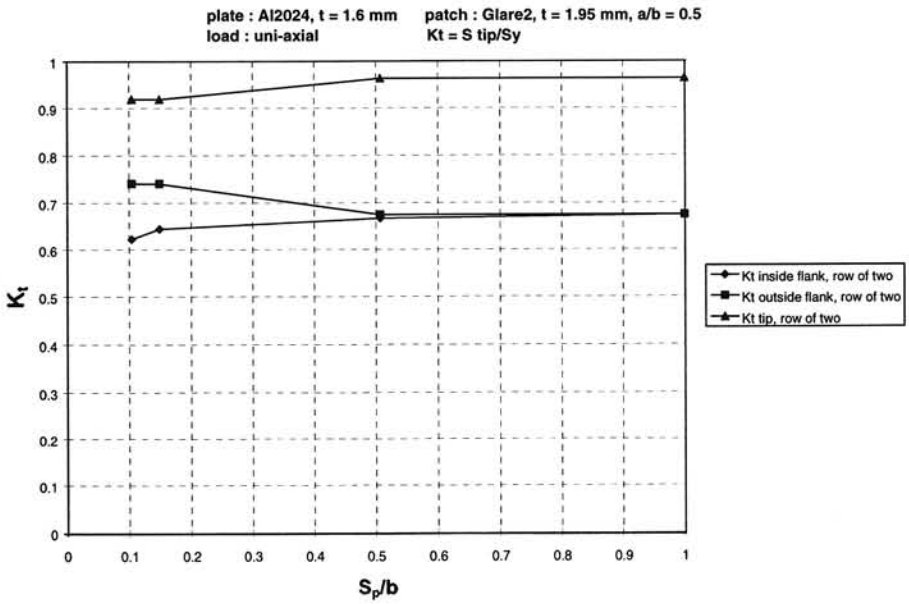

Figure 5.3: Skin stress concentrations in a row of two elliptical patches, a/b = 0

When considering an infinite row of circular patches, the results are similar. The stresses at the flanks and tips are lower at smaller patch separations (figure 5.4) and the stresses in the inclusion decrease as well, i.e. the stress decrease in the skin is not caused by more load attraction in the inclusion. In fact, the average plate thickness increases along the patch row with smaller patch separation, resulting in decreasing average stresses along the row.

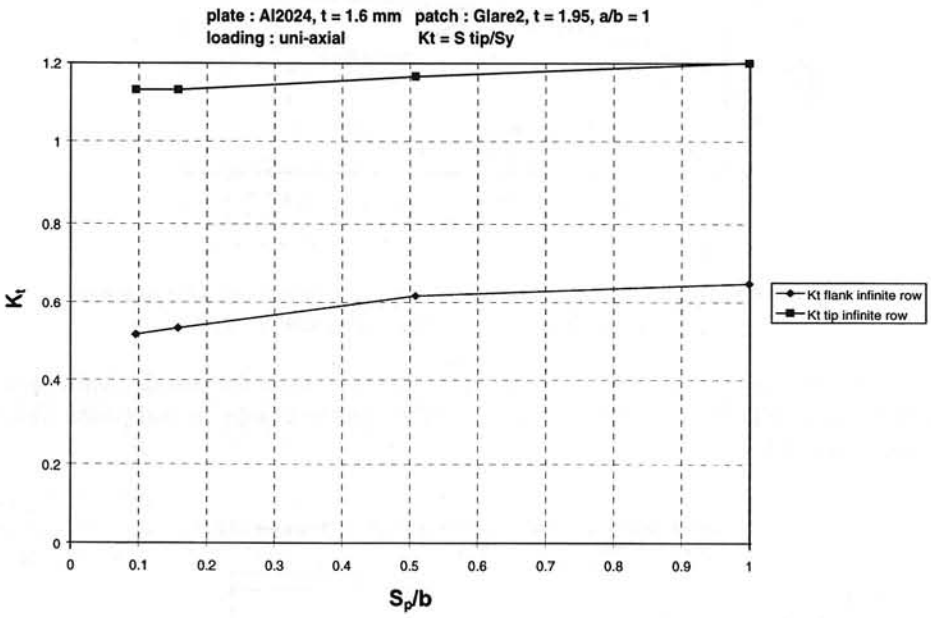

Figure 5.4: Plate stress concentration in an infinite row of circular patches [5.1]

Column of patches

A second situation that was considered, was a column of two patches. The highest stress concentration in the skin adjacent to a patch occurs at the patch tips. Therefore, one would expect more severe interaction effects in a column of patches at facing tips than in a row of patches at facing flanks.

A column of two patches was considered. Four elliptical patches with different aspect ratios were modeled. Figure 5.5 shows the stress concentration factors in the skin. 2D linear FE analysis showed a clear increase in stresses at the facing patch tips due to load attraction. As can be seen, for any of the four patches there is hardly any patch interaction for S_p/a ratios larger than 0.5. Below this value the increase of the tip stress concentration is considerable, especially when compared to a row of patches. Figure 5.5 also indicates that elliptical patches with high aspect ratios should be avoided in columns of patches.

Additionally, a square patch with small rounded corners was considered. This patch shape resulted in lower skin stresses when compared to an elliptical patch with the same aspect ratio. It can be concluded that if patch tip stresses are too high, an ellipse with flattened tips, an

octagon, or a rectangular patch can further decrease skin tip stresses. Due to strain compatibility, the load attraction will be spread along the patch width and therefore limit the peak stress.

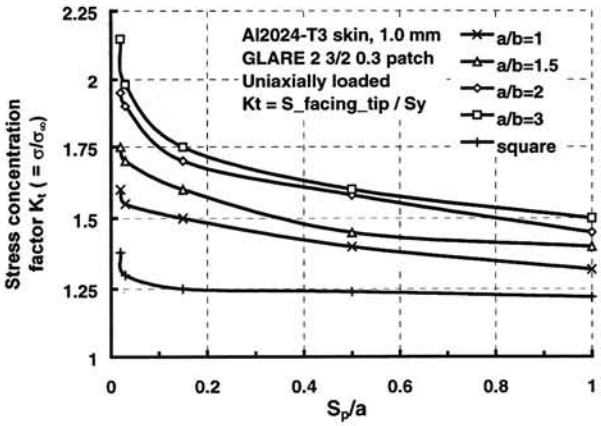

Figure 5.5: Influence of the distance between two patches on the stress concentration K_t at facing patch tips (a is half patch length, b is half patch width) [5.1]

In general it can be concluded that one should strive to combine the lowest possible patch aspect ratio with a patch separation ratio of at least 0.5 to achieve the minimum skin stress. Stress concentrations at the patch tips with an arbitrary shape due to patch interactions can be decreased in two ways:

- increasing the tip radius
- decreasing the patch length 2a

The previous discussion of a row and a column of patches was done for a uni-axial loading case. Tests under bi-axial loading with a barrel set up resulted in considerably lower tip stresses [5.3].

5.1.2 The influence of patch separation on secondary bending

Besides load attraction, there is another effect that contributes to the stress-increase in the skin at the patch tips. The consequences of secondary bending are often more severe than the consequences of load attraction. This is also the case when multiple patches are applied. Consider the configuration shown in figure 5.6.

Figure 5.6: Schematic representation of the neutral line in loading direction

As can be seen, there is an eccentricity in the neutral line when moving from one patch to the other. This eccentricity results in secondary bending stresses when loaded in the direction as given in figure 5.6. As the patch separation decreases, the skin between the two patches is

subjected to increasing bending stresses. In case of a short single patch, an inflexible part (skin and patch) is present between two flexible parts (the skin on both sides of the patch), but in the case of two patches next to each other, the flexible part is situated in between two stiffer parts. When the separation is small enough, the skin between the patches will act as a hinge.

The Neutral Line model (section 4.3) is used to obtain a numerical estimation of the magnitude of the bending stresses. The neutral line is divided in 5 parts with two different flexural rigidities (tapering is neglected). Three parts represent only skin and two parts represent a skin-patch combination. The influence of patch separation on secondary bending can now be determined. Figure 5.7 shows the bending stress as a function of the absolute patch separation for three different patch lengths (2a = 50, 100 and 200 mm).

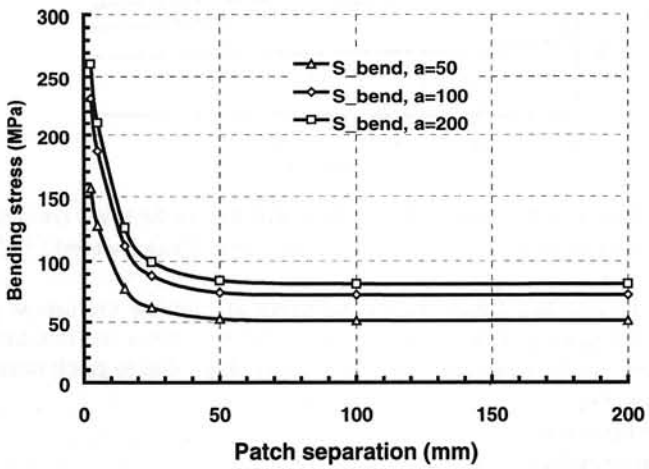

Figure 5.7: The influence of patch separation on skin bending stress at adjacent patch tips. Load attraction effects are included [5.1]

For all three patch lengths, the effect of secondary bending as an interaction effect clearly occurs for separations smaller than ~50 mm. Thus, secondary bending effects due to patch interaction are determined by absolute patch separation, contrary to load attraction effects that are determined by relative separation.

5.1.3 The influence of load attraction on secondary bending

Load attraction into the patched area will cause stress concentrations at the patch tips. Due to these higher tip stresses, the secondary bending along the patch centerline will increase. When the stress concentration at the patch tip is known, the effect on the secondary bending stress can be approximated with the neutral line model. This is done by substituting the tip stress for the applied stress in the model [5.4]. The results from this calculation are therefore only valid for the part of the neutral line in between and including the patch tips.

The increase of the tip stress due to load attraction is more severe for patches with higher aspect ratios (long slender patches). Therefore, the influence of the stress concentration on

secondary bending at the patch tip is larger for these patches (see figure 5.8). Since the neutral line model is a two-dimensional model, it does not account for the influence of the patch aspect ratio on secondary bending.

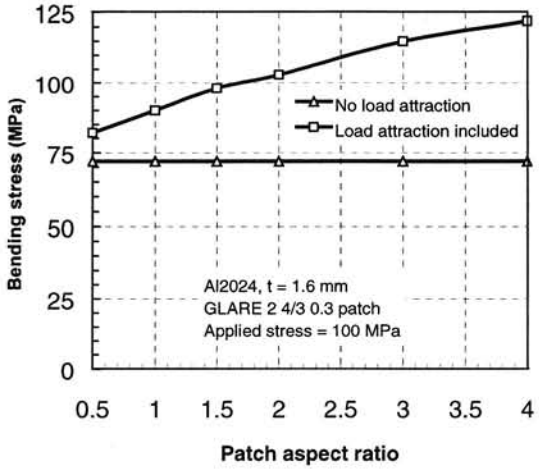

Figure 5.8: Secondary bending stresses versus patch aspect ratio (a/b)

5.1.4 The influence of taper ratio on secondary bending

In order to reduce the bending stresses in the skin and adhesive stresses at the patch tip, the edges of the patch are tapered. Tapering of patches will gradually change the neutral axis of the patch-skin combination and so decrease bending stresses. Figure 5.9 shows an example of a stepped tapering.

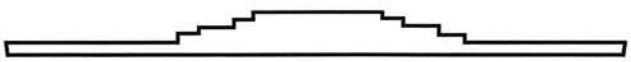

Figure 5.9: Schematic representation of a repair with tapered patch

CalcuRep® calculates the bending stresses using a patch thickness equal to the minimum taper thickness. This results in a bending stress that is lower than the maximum bending stress without taper. It is obvious that, by taking this minimum taper thickness as patch thickness, the maximum bending stresses are underestimated and it is interesting to know to what extend.

It is difficult to incorporate a continuous taper since the thickness of the patch-skin combination is not constant in the tapered region. This would result in a non-linear differential equation that is more difficult to solve. The tapering of boron patches is accomplished by stepping down the ply lengths and can be solved using the discrete step model. This model is also valid for GLARE® patches despite its continuous taper because the individual layers require a certain small length before they are fully loaded.

It is incorrect to assume that the taper step closest to the repaired structure determines the secondary bending in the skin, in order to use this minimum taper thickness to calculate the bending stresses. The remaining steps do affect the bending stresses at the patch tip (see figure 5.10). Although the individual moments originated at the eccentricity jumps are smaller compared to the untapered configuration, the moments M_3 to M_4 still significantly affect the moment at M_1.

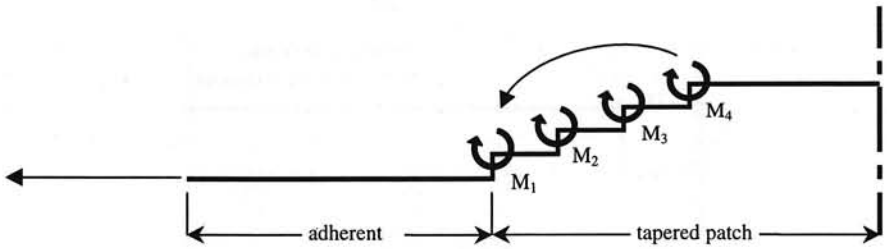

Figure 5.10: Secondary bending moments at the discrete steps of a tapered patch

To illustrate the effects of a realistic taper on secondary bending stresses, some calculations were performed for an untapered patch, tapered patch and a patch with a thickness equal to the minimum taper thickness. Three different patch configurations were analyzed [5.4], a GLARE2 3/2 0.3 patch on a 1 mm skin, a GLARE2 4/3 0.3 patch on a 1.6 mm skin and a 4-ply boron patch on a 1 mm skin. The results can be seen in figure 5.11.

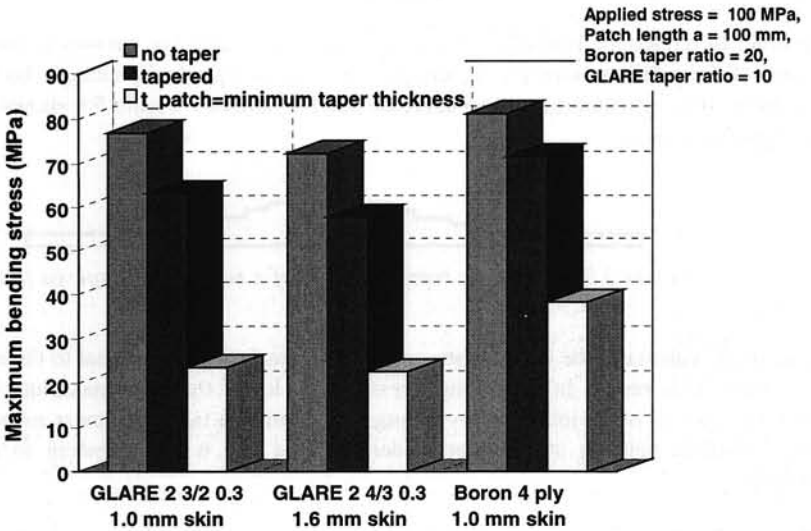

Figure 5.11: Bending stresses at the patch tip with respectively untapered patch, tapered patch, and patch thickness assumed equal to the minimum taper thickness [5.1]

The underestimation of the secondary bending stress when using a patch thickness equal to the minimum taper thickness, as incorporated in CalcuRep®, is apparently very large. Neglecting the taper in the NLM gives a better approximation than using the minimum taper thickness. A factor of 4 difference was found between the two extremes. The tapering results in a stress reduction in the order of 20% for a taper ratio of 1:10. With tapering, the load attraction reduces due to the smaller extensional stiffness. However, this reduction is only in the order of 2% for taper ratios of 1:10.

The same analysis was performed with a 4-ply boron/epoxy patch, a 3-ply boron/epoxy patch and a GLARE2 3/2 0.3 patch with different taper ratios. All three patch configurations were applied to a 1.0 mm Al 2024-T3 skin. This resulted in the following patch-skin extensional stiffness ratios: 1.52, 1.14 and 0.97 respectively. Taper ratios varied between 0 and 30. The result can be found in figure 5.12.

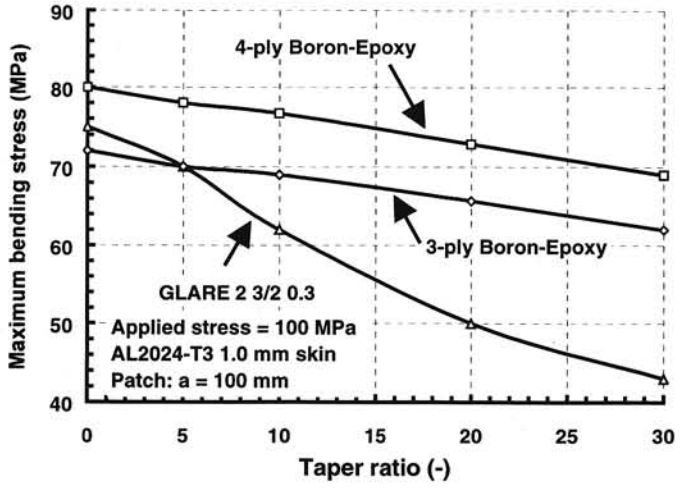

Figure 5.12: The influence of taper ratio on the maximum skin bending stress [5.1]

Tapering with a realistic ratio in the range from 1:10 to 1:20 results in a skin bending stress reduction between 10% and 35%. Thicker patches appear to benefit more from tapering than thin patches although $K_{t(bending)}$ values remain high, in the range from 1.5 to 1.75.

It can be concluded that when designs become critical at the patch tip, tapering can reduce the stress concentration. However, the effectiveness of the patch is reduced significantly and the bond line at the crack is loaded more severely in order to transfer the load. Keeping in mind the load transfer length of the patch, tapering can be quite successful to reduce the severity of the patch run out.

5.2 FEM calculations of stress intensity factors

Whereas the calculations in the previous paragraph were concentrated on the stresses in the periphery of a bonded repair, calculations have also been performed for the stress intensity factors at the crack tips using the Modified Crack Closure method. The following assumptions were made for the FE models:

- the plate contains a through crack in the center of the plate
- the patch is intact
- the plate is in plane stress conditions
- initial thermal effects due to curing are not accounted for
- the plate and patch do not contain imperfections
- the plastic zone at the crack tip is small compared to the crack size in order to allow usage of Linear Elastic Fracture Mechanics

The 3D model that was used as input for ABAQUS contains three layers; first layer is the panel, the second layer represents the bond line and the third layer represents the full-width patch. The panel and patch are modeled using 8-node reduced integration shell elements (S8R), the bond line is modeled with 20-node brick reduced integration elements (3D20R). These elements are necessary to enforce the right boundary conditions between the bond line and the panel and patch (according to Mindlin plate theory), and to be able to examine internal stresses, e.g. peel stresses, in the bond line. Debonds were modeled by not defining the boundary condition between the adhesive and the adherends. The dimensions of the specimen modeled can be seen in figure 5.13. The GLARE® lay-up used in this model was GLARE2 3/2 0.3.

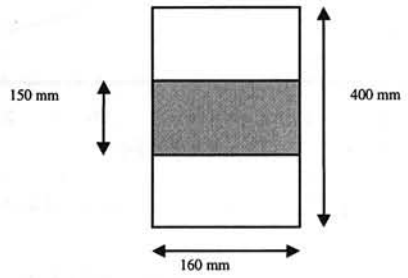

Figure 5.13: Dimensions as used in models
t_{al} = 1.2 mm, E_{al} = 72000 MPa, t_{GLARE} = 1.4 mm, t_{ad} = 0.13 mm, σ = 120 MPa

Three influences were investigated:

- The influence of bending on the stress intensity factor K
- The influence of debonds on the stress intensity factor K
- The influence of different GLARE® patches on the stress intensity factor K

5.2.1 The influence of bending on the stress intensity factor K

Using the model described in the previous paragraph, the influence of secondary bending on the stress intensity factor was studied. Figure 5.14 shows the stress intensity factor K_{mid} (K_{mid} is the stress intensity in the middle of the repaired skin) for the case with bending compared to the stress intensity K without bending. As can be seen, bending has a large influence on the stress intensity and can therefore not be neglected.

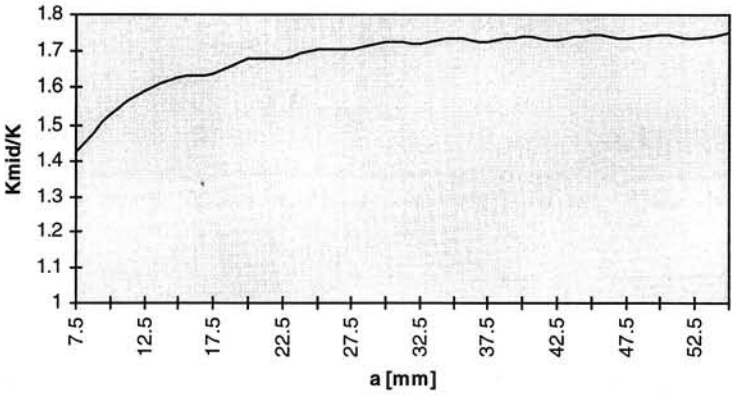

Figure 5.14: Comparison of FEM results with bending to results without bending [5.5]

The results have been compared to two theoretical methods; the method developed by Ratwani and the method developed by Wang, Rose and Callinan [5.6]. This second method defines an upperbound of 18.5 MPa$\sqrt{m}$ for K whereas Ratwani's method results in an increasing K for increasing crack length. Figure 5.15 shows this comparison and also some experimental results where K was measured with strain gauges [5.7]. The strain gauges were positioned after the curing process so the measured K did not include residual thermal stresses, as was the case for the FE models. The experiments resulted in a nearly constant K value of 10.2 MPa$\sqrt{m}$ with an accuracy of $\pm$ 5%.

It can be seen that the FE model predicts an upperbound value for K. Possible reason for the large overestimation of the theoretical upperbound value (factor of 1.8 difference) is that this theory assumes a quasi-isotropic material and plane strain conditions, two factors that are not present in the FE model since GLARE2 3/2 0.2 is highly anisotropic. The theory of Ratwani seems to give better agreement with the FE results. As can be seen from figure 5.15, there is a fairly good comparison of the FEM results and the experiments at larger crack sizes.

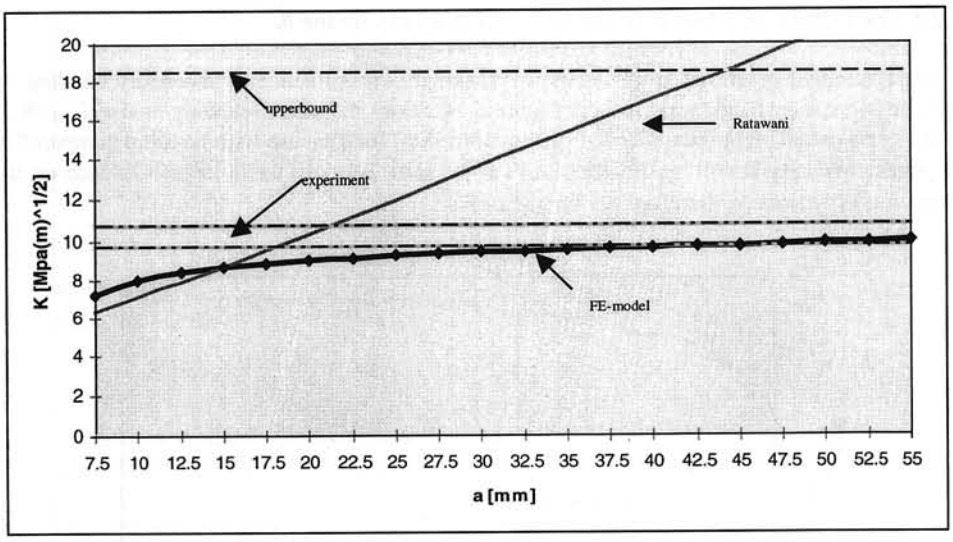

Figure 5.15: Results of analyses and experiments with bending [5.5]

The remaining question is whether there is an upperbound for K in the case with secondary bending. The FE results seem to indicate such an upperbound. As can be seen from figure 5.15, the stress intensity factor is almost constant for crack lengths where a is larger than 22.5 mm.

5.2.2 The influence of debonds on the stress intensity factor K

Calculations with debonds were done at two different crack lengths, a = 22.5 mm and a = 50 mm. For reasons of simplicity, debonds were assumed to be rectangular of shape, reaching as far as the crack tip. Four different debond heights were examined; b = 0.5 mm, b = 1.0 mm. b = 1.5 mm, b = 2.0 mm. Figure 5.16 shows the results of the calculations. Three different K values can be seen; K_b is the stress intensity due to pure bending, K_{mid} is the stress intensity in the middle of the repaired plate and K_{max} is the maximum stress intensity factor (= K_{mid} + K_b). As can be seen, the stress intensity due to pure bending is independent of debond height. As a consequence, an increase of the maximum stress intensity K_{max} is only caused by an increase of K_{mid}.

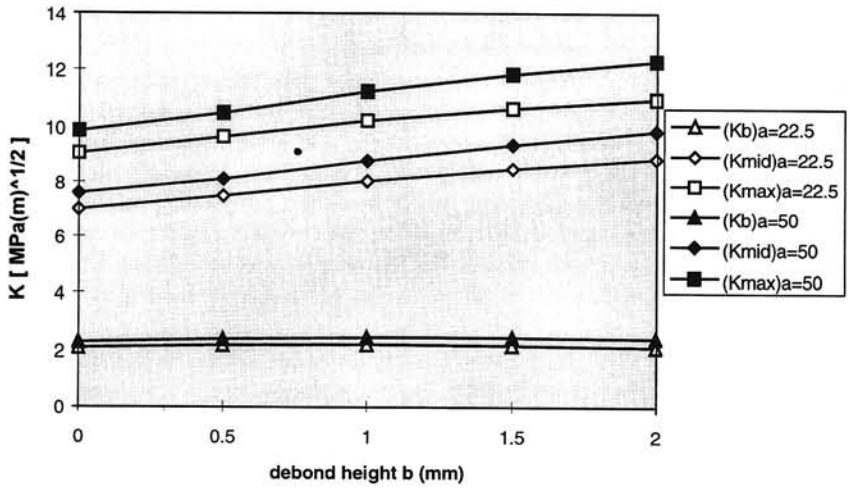

Figure 5.16: Influence of debonds on K-factors (with bending) at two crack lengths : a = 22.5 mm and a = 50 mm [5.5]

5.2.3 The influence of different GLARE® patches on the stress intensity factor K

The influence of the thickness of GLARE® patches on the stress intensity factor was examined by modeling four different materials in the FE models. The lay-ups were all GLARE2: 2/1 (t = 0.85) mm, 3/2 (t = 1.4 mm), 4/3 (t = 1.95 mm), 5/4 (t = 2.5 mm), 6/5 (t = 3.05 mm). The results can be seen in figure 5.17. As can be seen, a thicker patch results in a lower stress intensity factor, the bending stress is reduced by using a thicker patch. For a thickness larger than 1.95 mm, the relative reduction of K becomes small.

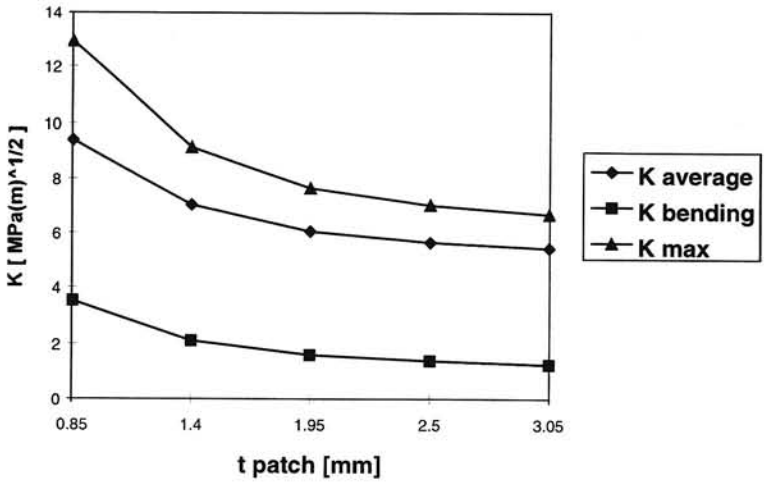

Figure 5.17: Influence of patch thickness on K, bending included (a=22.5 mm) [5.5]

5.3 Conclusions

From this chapter, the most important conclusions are:

- When applying columns of patches in close proximity, high stresses at the facing patch tips may lead to dangerous situations. Since fairly good estimates can be made of the facing tip stress using finite element calculations or the extended Rose model, this repair configuration does not need to be avoided; care should be taken to maintain a certain minimum separation between the facing tips in a column of elliptical patches, in order to keep the tip stress at an acceptable level. Flank stresses of facing flanks for rows of patches under bi-axial loading were not critical. Furthermore, it was found that a bi-axial stress field has a favorable effect on the stress at the patch tip, compared to the uni-axial situation.
- The increase of the tip stress due to load attraction is more severe for patches with higher aspect ratios (long slender patches). Therefore, the influence of the stress concentration on secondary bending at the patch tip is larger for these patches.
- It can be concluded that when designs become critical at the patch tip, tapering can reduce the stress concentration. Keeping in mind the load transfer length of the patch, tapering can be quite successful to reduce the severity of the patch run out.
- Secondary bending has a large influence on the stress intensity factor and can therefore not be neglected.
- According to FE results, debonds can have a significant effect on the stress intensity factor.

[5.1] Ipenburg, G., *Analysis of Stresses in the Periphery of Bonded GLARE Repair Patches*, Master Thesis, Delft University of Technology, The Netherlands, June 1997.

[5.2] Lekhnitskii, S.G., *Anisotropic Plates*, Gordon and Breach Science publishers, New York, 1968.

[5.3] Siwpersad, D.R.C., *Bonded GLARE Patches for the Repair of Cracked Aluminum Fuselages*, Master Thesis, Delft University of Technology, The Netherlands, December 1996.

[5.4] Fredell, R.S., Müller, R.P.G., *Analysis of Multiple Bonded Patch Interaction*, Proceedings 4th USAF Aging Aircraft Conference, Colorado Springs, July 1996.

[5.5] Massar, J.J.A., *Calculation of stress intensity factors of a bonded repair by means of a finite element method*, TZ Report, Delft University of Technology, The Netherlands, July 1998.

[5.6] Wang, C.H., Rose, L.R.F., Callinan, R., *Analysis of out-of-plane bending in one-sided bonded repair*, Int. J. Solids Structures Vol. 35 N.14 pp. 1653-1675, 1998.

[5.7] Nijssen, P.J.M., *Qualitative Investigation of Disbond Mechanisms under Single-Sided Adhesively Bonded Repairs,* Master Thesis, Delft University of Technology, The Netherlands, December 1997.

CHAPTER 6

IN-SERVICE EFFECTS ON PATCH PERFORMANCE

In general it can be said that the design and application of bonded repairs is well understood. One field where questions are still unanswered is the behavior of bonded repairs subjected to in-service conditions. This chapter will focus on two in-service effects, debonds [6.1] and thermal effects [6.2], that might influence the performance of bonded repairs.

6.1 The influence of debonds on patch performance

Research showed that the debond mechanism is not static, but caused by fatigue of the adhesive [6.2]. C-scans of bonded repairs confirmed that debonds grow gradually in the wake of the crack tip. A minimum crack length, and therefore strain in the adhesive, is necessary for debonds to occur. Cycles applied before reaching this crack length do not influence the development of debonds and the debonds did not cause sudden changes in crack growth rate.

The effects of artificial debonds on the fatigue response of cracked aluminum panels repaired with GLARE® and boron/epoxy patches was investigated [6.1]. The debonds were created by using Teflon inserts. Four artificial debond types were defined (figure 6.1).

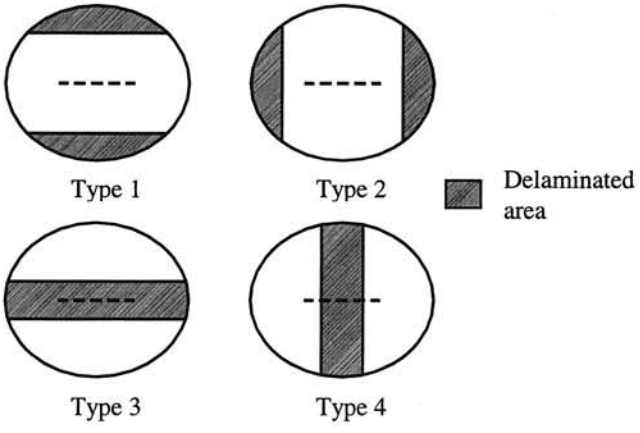

Figure 6.1: Artificial debonds

Depending on the debond type, debonds can have the following effects:

- Reduced effectiveness of the patch
- Higher shear strains
- Degraded durability
- Less load attraction, influencing the skin stress and $K_{repaired}$

The repairs were made according to the following specifications:

- Specimens pre-cracked, length 25 mm, no stop-drill
- Uniaxial loading
  6-120 MPa for the GLARE® repairs
  12-120 MPa for the boron/epoxy repairs
- Cure temperature 120 degrees Celsius (250 degrees Fahrenheit)
- Patch size (optimized by material)
  50 mm long x 60 mm wide GLARE® patches
  70 mm long x 50 mm wide boron/epoxy patches
- Patch ≈1/3 full specimen width to allow important 2D load transfer

Figure 6.2 shows the effects on crack growth of the different types of debonds that can occur for bonded GLARE® repairs. As can be seen, most types of debonds caused a decreased re-initiation period after bonding. Debonds of type 2 and 4 had about the same crack growth rate as a repair without debonds. A debond of type 3 resulted in crack growth immediately after repair and had a larger crack growth rate. Debonds of type 1 showed an increased crack growth life compared to the repair without debonds. Due to the debonded patch tips, the effective length of the patch is smaller, reducing the load attraction by the patch. This results in a lower K at the crack tip and thus a lower da/dn.

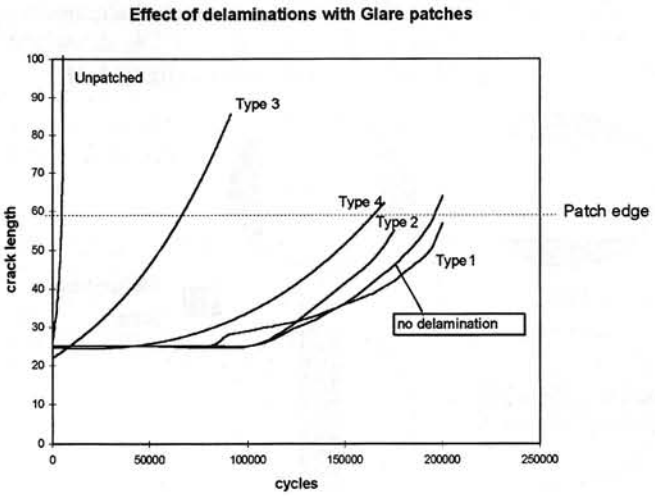

Figure 6.2: The effects of the different types of debonds on crack growth under GLARE® patches [6.1]

Figure 6.3 shows that boron repairs performed less well with delaminations of the same type as GLARE® repairs although it must be said that da/dn for boron is higher in the first place.

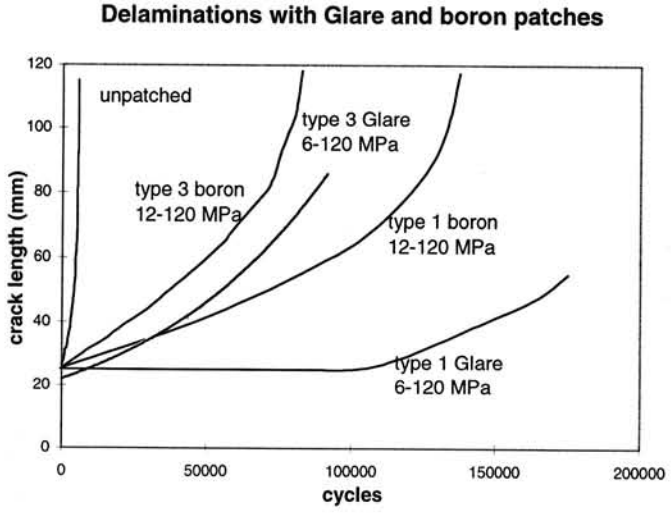

Figure 6.3: Comparison of delamination effects for GLARE® and boron repairs [6.1]

Concluding from figure 6.2 and 6.3 one can say that:

- Type 1 (patch tip disbonds): The shorter effective patch can reduce K due to less load attraction. May be hurt by freeze/thaw cycles.
- Type 2 (patch edge disbonds): There is a constant K under the patch, little effect on crack growth.
- Type 3 (crack flank disbond): There is more crack opening resulting in the highest K and thus, highest da/dn. Expected to be most important after the application of peakloads.
- Type 4 (center vertical disbond): Act as two patches over the crack tips, little effect on crack growth.

The previous shows that delaminations can have an effect on crack growth. Delaminations of type 3 show to be most harmful for crack growth under the patch. Although debonds of type 3 occur in actual fatigue testing, these debonds stay well behind the crack tip, resulting in less influence as was seen here. Damage tolerance is assured because crack growth remains small, which makes detection during inspection possible. The data provides a starting point for defining bonded repair inspection intervals to detect bondline defects.

6.2 Thermal effects

The second in-service effect that will be discussed here are the effects of different thermal exposures on patch performance. The results of two different exposures will be shown here; thermal cycling and isothermal low temperature tests. The first paragraph will describe the specimens, the following paragraphs will describe the tests and results.

6.2.1 Description of the specimens, manufacturing and test equipment

Description of thermal specimens
The panels used in the thermal tests have an initial crack length of 25 mm and were pre-cracked at 60-3 MPa. The panels are Al 2024-T3 clad, width is 180 mm, length is 400 mm and thickness is 1 mm. For both the boron and GLARE® patches, the patch width is one third of the panel width.

Before pre-cracking, a hole was drilled in the center of the panel from which a saw cut was made with a total length of 20 mm. The panels were all pre-cracked to 25 mm at a frequency of 10 Hz. The specimens can be seen in figure 6.4 and 6.5.

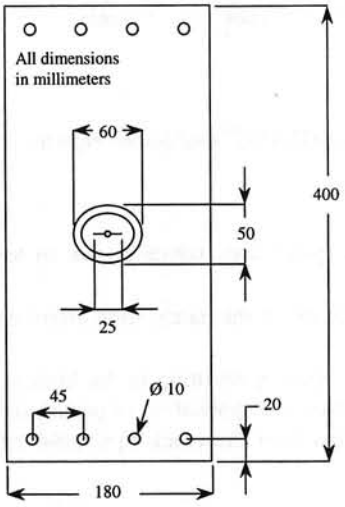

Figure 6.4: Thermal specimen with GLARE® patch

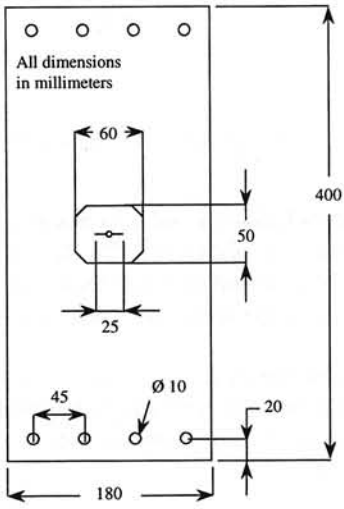

Figure 6.5: Thermal specimen with boron patch

Description of the patches
The GLARE® patches were all made of GLARE2 3/2 0.2, 3 layers of aluminum and 2 layers of glass-epoxy prepregs, with a total thickness of 1.1 mm. To prevent high skin stresses and adhesive peel stresses, the edges of the GLARE® patches were tapered. The taper width was 7 mm. The patch was tapered up to a minimum thickness of 0.2 mm, which is the thickness of the bottom aluminum layer. A close-up of the taper is given in figure 6.6. The taper was CNC-milled in twenty equal steps. Since GLARE2 is a uni-directional material, i.e. the fibers are in one direction, the fiber direction of the patch was perpendicular to the crack.

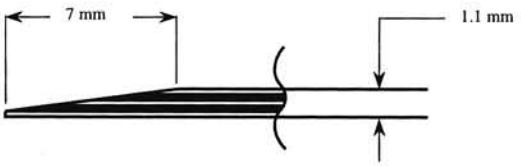

Figure 6.6: Close-up of taper of GLARE® patches

The boron patches consist of three boron-epoxy plies. The boron/epoxy was made by Textron Specialty Materials, 5521/4, with a thickness of 0.13 mm per ply, resulting in a patch thickness of 0.39 mm. This lay-up was chosen to keep the extensional stiffness (E_t) as close as possible to the extensional stiffness of the GLARE® patches (80730 N/mm for boron patches versus 75900 N/mm for GLARE® patches).

An inverted wedding cake lay-up was used, i.e. the largest ply is on the outside of the repair and the smallest ply is closest to the specimen. Tapering of the boron patches, in order to reduce stresses in the skin and adhesive at the patch tip, is accomplished by stepping down the length of the plies. The dimensions are given in figure 6.7.

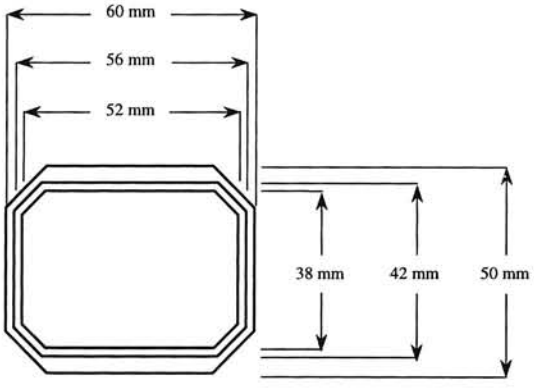

Figure 6.7: Dimensions of the boron patches

Pretreatment of the specimens
The specimens were pretreated with the P2 surface preparation method. After the pretreatment, the specimens were primed, using BR-127 from Cytec. More about the P2-etching can be found in [6.3].

Bonding of the patches
For bonding, AF-163-2M (0.06 lbs/sqft) adhesive from the 3M company was used. This is an epoxy based film adhesive with a nylon mat carrier. The carrier is to assure a minimum thickness of the adhesive layer after curing. After positioning the patches on the panels, the patches were taped at the edges with polyamide tape to prevent shifting when the temperature is increased and the adhesive becomes liquid. The adhesive was cured using a Briskheat ACR9000A ramp programmable controller.

The following cure cycle was used (see figure 6.8):

- Apply full vacuum pressure, approximately 20 inch Hg.
- Increase temperature from room temperature to 50°C at a rate of 2°C per minute
- Soak at 50°C for 30 minutes
- Decrease vacuum pressure to 12 inch Hg.
- Increase temperature to 120°C at a rate of 2°C per minute
- Soak for 1 hour at 120°C, for every degree lower in temperature, the soak time has to be increased with 0.175 hour.
- Cool down at a rate of 2°C per minute, the vacuum can be reduced below 70°C.

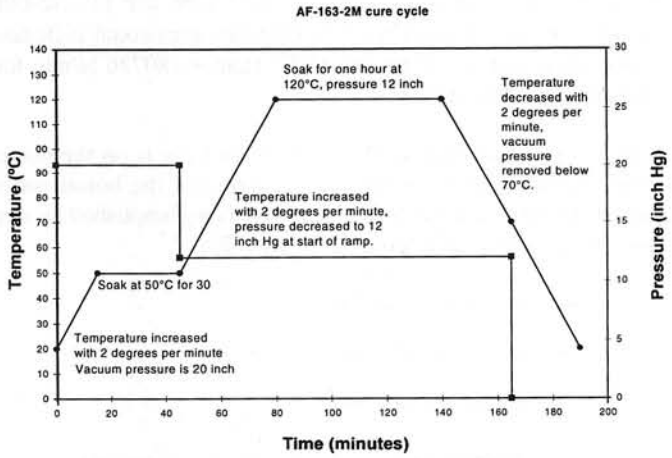

Figure 6.8: The AF-163 cure cycle used for bonding patches

Thermal cycling equipment

The thermal cycling was performed using a dual chamber thermal cycling machine manufactured by Rusell's Technical Products (Holland, MI). The cycling is performed at Warner Robins Air Logistics Center, Robins Air Force Base in Georgia.

The machine consists of two thermal chambers on top of each other. The top chamber was kept at the maximum cycle temperature of +80°C using electric heating elements, the bottom chamber was kept at the minimum cycle temperature of -40°C. The specimens are placed on a tray and moved between the two chambers using an automatic pneumatic trolley mechanism. All specimens are stacked together, with an air gap between each specimen. A thermocouple is attached to the center specimen. It takes 10 minutes to ramp down from +80°C to -40°C and 6 minutes for the reverse cycle, resulting in a total cycle time of 16 minutes where the specimens are guaranteed to be kept at the maximum and minimum temperature for at least 30 seconds.

The configuration of the chamber does not allow fatiguing the specimens at the same time as the thermal cycling takes place. Only thermal effects due to the difference in thermal expansion coefficient and the resulting thermal stresses can be monitored. Different thermal cycling equipment, capable of fitting around a fatigue test frame is needed to simulate a true

GAG cycle. The disadvantage of this equipment is that it is slower and uses more energy and liquid nitrogen.

Isothermal equipment

The thermal chamber used for the isothermal, high and low temperature exposures, is a Bemco Inc. (Simi Valley, California) thermal chamber. For the low temperature exposures, the chamber was placed around the specimen during fatigue testing. The test set-up is given in figure 6.9. A thermocouple at the center specimen registered the actual temperature of the specimens.

Figure 6.9: Test set-up for isothermal low temperature tests

Fatigue machine

The fatigue machine used in this project is a MTS® hydraulic fatigue machine. The load frame has a capacity of 500 kN, the load cell has a capacity of 250 KN. The machine is controlled by a Teststar™ II control system. A traveling microscope is mounted on the load frame in order to check crack growth during testing. All tests, except for the spectrum tests, were performed at 10 Hz.

C-scan equipment

The C-scan used is a Panametrics Multiscan Inspection System. The software used is version 6.00 (released January 1996). The system consists of a water tank with a C-scan mechanism, which allows scanning motion of the transducer and receiver, figure 6.10.

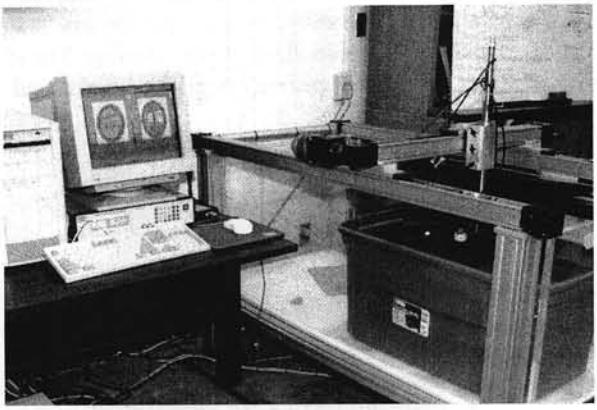

Figure 6.10: C-scan equipment

Bonding equipment

For the bonding of the patches, a Briskheat ACR9000A ramp programmable controller was used, see figure 6.11.

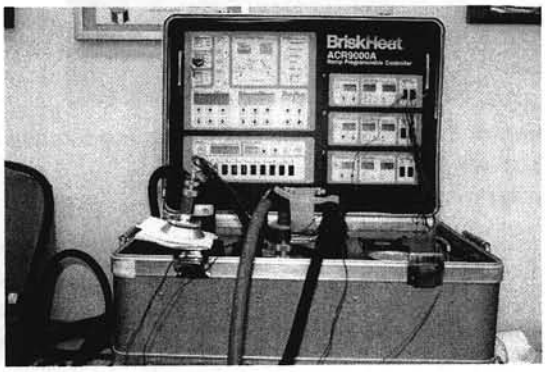

Figure 6.11: Briskheat hotbonder equipment

6.2.2 Thermal cycling tests

According to Baker [6.4], one of the most serious considerations regarding thermal residual stresses is thermal fatigue of the adhesive. When simulating a ground-air-ground (GAG) cycle, the thermal stresses in the bondline will change continuously and possibly cause thermal fatigue of the adhesive.

Besides the influence of the thermal cycling on the thermal residual stresses in the bondline, it is interesting to see if the temperature changes would cause degradation of the adhesive itself. Research has been done before on the effects of thermal cycling during fatigue testing by the Institute for Aerospace Research (IAR) in Canada and the Aeronautical and Maritime Research Laboratories in Australia (AMRL) [6.5]. The conclusion of this research was that the thermal cycling can have significant influence on the fatigue performance of bonded repairs. The specimens in the described program were thermally cycled during fatigue loading, which is not the case for the work described in this report.

The first thermal experiment consisted of thermal cycling of the specimens to simulate a ground-air-ground (GAG) cycle. During the thermal cycling, the specimens were unloaded. A GAG cycle from -40°C to +80°C was simulated. The thermal cycling will change the stresses continuously and possibly cause thermal fatigue of the adhesive. Not only mechanical damage is possible, also some chemical deterioration can take place, influencing the efficiency of the repair. Butkus [6.6] found that the properties for two types of epoxy-based adhesives degraded after thermal cyclic exposure.

Although the specimens had some kind of restraint while in the thermal cycling machine, see figure 6.12 [6.7], there was still some possibility for deformations out of plane, limiting the thermal stresses in the bondline.

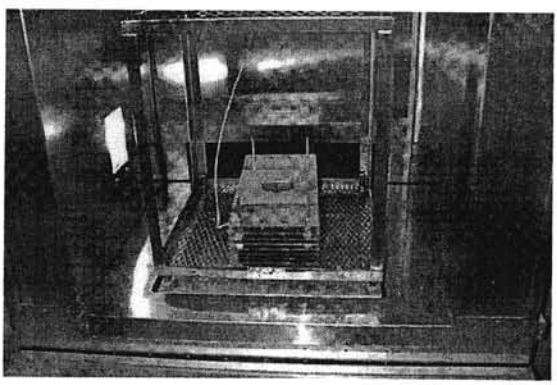

Figure 6.12: Specimens in thermal chamber at Warner Robins ALC [6.7]

A more realistic loading is the combination of thermal cycling with fatigue loading of the specimens, this was not possible here due to equipment limitations. To see whether thermal fatigue is of influence on the efficiency of the repair, a total of 8 tests were performed, see table 6.1.

The two different patch materials were chosen to look for differences in possible thermal fatigue, caused by the differences in thermal residual stresses in the bondline between boron and GLARE®. During testing, crack-growth data was obtained to construct crack-growth curves. The results can be seen in figure 6.13.

Specimen #	Initial crack length (mm)	Pre-crack level (MPa)	Fatigue level (MPa)	Patch material/ dimensions (mm)	Number of thermal cycles
T5	25	60-3	120-6	GLARE®, 60x50, ellipse	200 cycles, -40 to +80°C
T6	25	60-3	120-6	GLARE®, 60x50, ellipse	400 cycles, -40 to +80°C
T7	25	60-3	120-6	GLARE®, 60x50, ellipse	600 cycles, -40 to +80°C
T8	25	60-3	120-6	GLARE®, 60x50, ellipse	800 cycles, -40 to +80°C
T9	25	60-3	120-6	boron, 60x50, octagon	200 cycles, -40 to +80°C
T10	25	60-3	120-6	boron, 60x50, octagon	400 cycles, -40 to +80°C
T11	25	60-3	120-6	boron, 60x50, octagon	600 cycles, -40 to +80°C
T12	25	60-3	120-6	boron, 60x50, octagon	800 cycles, -40 to +80°C

Table 6.1: Test program for thermal fatigue tests

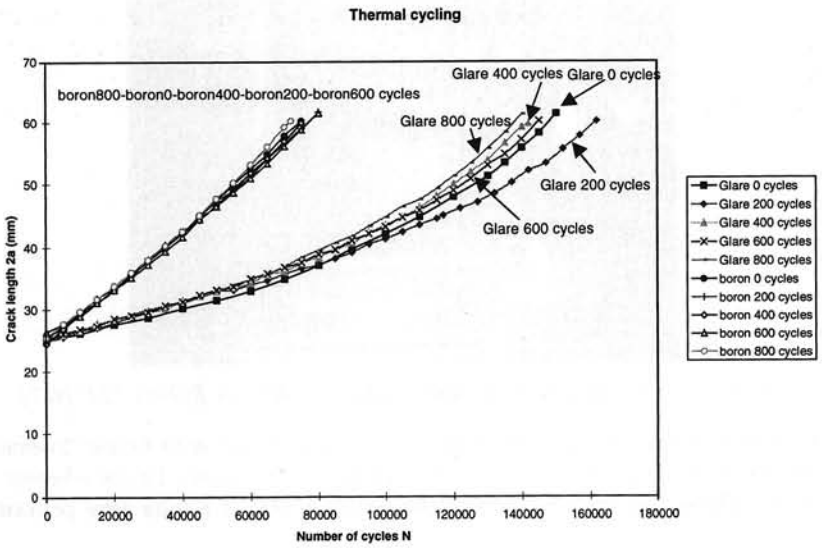

Figure 6.13: Crack growth curves of thermally cycled specimens [6.2]

As can be seen in figure 6.13, the specimens with the boron patches showed linear crack growth curves, the GLARE® specimens showed more parabolic crack growth curves. Crack growth rates were higher for the boron patches, no re-initiation period was found for the specimens, due to the low pre-crack stress level of 60 MPa.

The tests showed that for specimens with boron patches there is no effect of thermal cycling, i.e., crack growth behavior was similar to the non-cycled specimen. Specimens with GLARE® patches showed no effect of thermal cycling at smaller crack sizes. At larger crack lengths, small differences in crack growth towards the patch edge were observed, probably due to scatter in the results.

Although Butkus found degraded properties for two types of epoxy-based adhesives after thermal cyclic exposure, it can be concluded that thermal cycling does not cause significant changes in the fatigue properties of the bonded repairs that were tested.

6.2.3 Isothermal low temperature tests

Specimens were loaded in fatigue at low temperatures, simulating high altitude cruise flight, to see whether possible changes in adhesive properties might affect the repair performance.

Adhesives might perform less good at low temperatures compared to ambient temperatures, according to Butkus [6.6]. A problem that can occur at low temperatures is adhesive embrittlement. Adhesives can show a significant drop in fracture toughness at low temperatures. Additional tensile thermal stresses at -40 °C can also increase crack growth rates.

On the other hand, at low temperatures, the adhesive can become stiffer, resulting in less crack opening and less crack growth. Exposure of FM-73 to -40°C increased the shear modulus from 503 MPa to 791 MPa, possibly resulting in decreasing crack growth rates caused by reduced crack opening and thus a decrease in stress intensity factor. Another favorable effect is the decrease of crack growth rate in the aluminum caused by the lower temperatures. Crack growth tests on Al 2024-T3 sheets at -35°C showed a reduction in fatigue crack growth rate up to six times, depending on crack length [6.8].

The tests performed at low temperatures are given in table 6.2.

Specimen #	Initial crack length (mm)	Pre-crack level (MPa)	Fatigue level (MPa)	Patch material/ dimensions (mm)	Environmental exposure
G1	25	60-3	120-6	GLARE®, 60x50, ellipse	-40°C during testing
G2	25	60-3	120-6	GLARE®, 60x50, ellipse	-40°C during testing
B1	25	60-3	120-6	boron, 60x50, octagon	-40°C during testing
B2	25	60-3	120-6	boron, 60x50, octagon	-40°C during testing

Table 6.2: Test program for isothermal low temperature exposure during testing

Figure 6.14 shows the crack growth curves for the specimens tested at -40°C. As can be seen, the specimens with boron patches tested at low temperature show an increase of the fatigue life. Crack growth rates right after the start of the test are lower than for the specimen tested at room temperature. When looking at the crack growth curves for the specimens with GLARE® patches, the differences become even more significant. A large decrease in slope can be seen, indicating decreased crack growth rates.

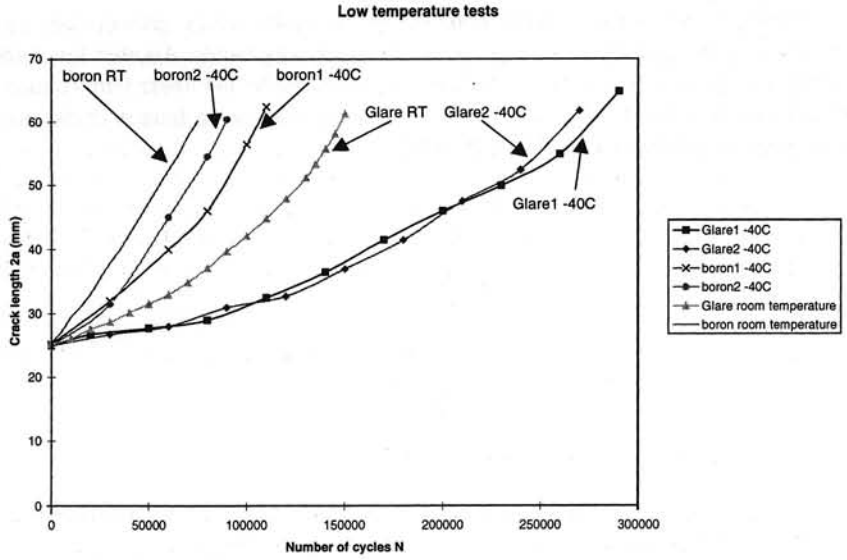

Figure 6.14: Crack growth curves of isothermal low temperature specimens [6.2]

Apparently, the change in adhesive stiffness and the reduced crack growth rates for aluminum at lower temperatures, and thus less water vapor in the air, overrule the detrimental effects of adhesive embrittlement and increased tensile thermal stresses.

6.3 Conclusions

The most important conclusions of this chapter are:

- Depending on the type of debonds they can result in a reduced patch effectiveness, higher shear strains, degraded durability and less load attraction.
- Thermal cycling before fatigue loading had no effects on patch performance for both boron-epoxy and GLARE® patches.
- Fatigue tests at -40°C resulted in significantly lower crack growth rates under both boron-epoxy and GLARE® patches. This is probably caused by the lower water vapor contents and an increased adhesive stiffness at lower temperatures, which overrule possible detrimental effects of adhesive embrittlement.

[6.1] Guijt, C.B., Fredell, R.S., CAStLE, USAFA, Colorado, *Delamination Effects in Fuselage Crack Patching*, Proceedings 41st International SAMPE Symposium, Anaheim, California, 1996.

[6.2] Verhoeven, S., *In-Service Effects on Crack Growth under Bonded Composite Repairs*, Master Thesis, Delft University of Technology, The Netherlands, July 21st, 1998.

[6.3] ASTM Design: E864-84, page 663.

[6.4] Baker, A.A., *Boron Fibre Reinforced Plastic Patching for Cracked Aircraft Structures*, Aeronautical Research Laboratories, Defence Science and Technology Organisation, Department of Defence, Aircraft, September 1981.

[6.5] Raizenne, M.D., Benak, T.J., Heath, J.B.R., Simpson, D.L., Structures, Materials and Propulsion Laboratory, Insitute for Aerospace Research, National Research Council of Canada, Ottawa, Canada, Baker, A.A., Department of Defence, Defence Science and Technology Organization, Aeronautical and Maritime Research Laboratories, Melbourne, Australia, *Bonded Composite Repair of Thin Metallic Materials: Variable Load Amplitude and Temperature Cycling Effects.*

[6.6] Butkus, L.M., *Environmental Durability of Adhesively Bonded Joints*, PhD Thesis, Georgia Institute of Technology, September 1997.

[6.7] Photos by Jerry Rowell, Warner Robins ALC.

[6.8] Broek, D., *Residual Strength and Fatigue Crack Growth in Two Aluminium Alloy Sheets at Temperatures Down to -75 °C*, NLR Report TR 72096, 1972.

CHAPTER 7

APPLICATION AND QUALIFICATION OF A BONDED GLARE® REPAIR ON THE C-5A GALAXY

7.1 Introduction

The first prototype application of GLARE® was the installation of two bonded patches on the aft crown section of a C-5A Galaxy transport aircraft, largest in the U.S. military fleet, in 1995. The C-5A fleet, with an average age of 27 years, suffers from multiple small cracks in the aft upper crown section of the fuselage.

Due to the large tail section of this aircraft, in combination with negative tail loads in flight, high tensional stresses occur in the aft crown section. The fuselage skin, Al 7079-T6, is very sensitive to stress corrosion, and cracks with a length of 25 to 50 mm occurred in the upper crown section. Most cracks nucleated from rivet holes due to high fit-up stresses induced by manufacturing. Riveted repairs were unsuccessful; new cracks initiated at the corner rivets of the patch. The only alternative besides re-skinning the cracked area was the application of bonded repairs, which is a more cost-effective solution. The repair can be seen in figure 7.1.

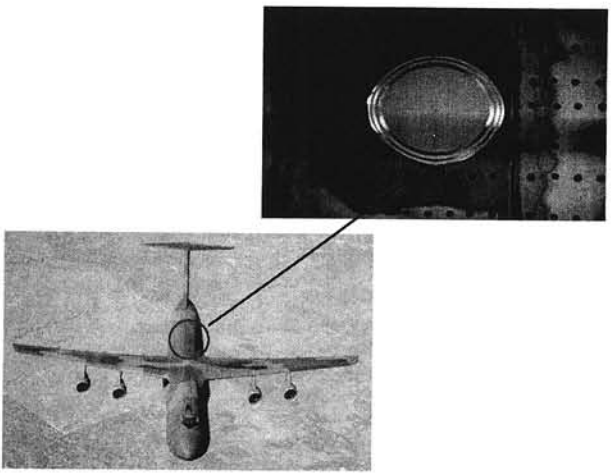

Figure 7.1: GLARE® patch on C-5A Galaxy

7.2 Preliminary testing and design

Before the decision was made to use GLARE® patches, a parametric study was done, involving several other patch materials such as boron/epoxy and carbon/epoxy. Based on this study, boron/epoxy and GLARE® were continued into the experimental phase.

Constant amplitude fatigue tests were carried out on 2024-T3 aluminum panels. These tests showed better performance for the GLARE® patches [7.1]. The better performance of the GLARE® repairs was attributed to the smaller CTE mismatch with the parent material. In addition to these tests, two tests were performed on 7079-T6 panels, taken from an operational C-5A. These tests showed that the GLARE® patches were able to prolong the life of the cracked panels significantly. Therefore, it was decided to use GLARE® for the C-5A prototype repair. The repairs were designed using CalcuRep®.

7.3 Installation

In October 1995, specialists from San Antonio ALC, Wright Laboratory and the US Air Force Academy installed two bonded GLARE® patches on a cracked C-5A fuselage.

A thermal survey of the repair locations identified temperature fluctuations not greater than 10°C. Cure times were adjusted to match the lowest cure temperature. An ACR-6000A computer controlled hot bonding unit monitored and adjusted the heating.

After the thermal survey, the surface was pretreated. A silane surface preparation technique was applied, involving:
1. grit blasting the aluminum skin,
2. cleaning the skin with an organic solvent,
3. applying a silane adhesion promoter, and
4. priming and curing with an epoxy adhesive primer

The patches were first printed on paper and then transferred to the sheet material. The elliptical shapes were then cold-rolled to match the diameter of the fuselage. A shear cutter was used to cut the patch to the rough dimensions, and a belt sander was used to trim the patch to the final outer dimensions.

The patch was tapered to decrease secondary bending. The minimum taper thickness was 0.3 mm, the taper angle approximately 1:10. If the minimum taper thickness is taken too small, the ability to produce a good bond fillet is reduced and the risks of damaging the edge of the patch are increased. After manufacturing to the proper shape, cleaning/degreasing the patch with a solvent as MEK is sufficient to prepare the patch for bonding since GLARE® is pre-primed.

After the surface preparation and patch manufacturing were complete, the area to be bonded was kept free of contaminations by covering and sealing it with a plastic film. The patch was bonded to the fuselage using AF-163-2M (3M) and a cure cycle of 125°C for one hour. A vacuum bag was used to apply a pressure of 50 kPa (15 inches of mercury). After bonding, the bondline and crack can be monitored using several different techniques such as eddy current or pulse-echo ultrasonic methods.

7.4 Qualification of a bonded repair to C-5A fuselage cracking under spectrum fatigue loading

The effectiveness of bonded GLARE® patches was already investigated using constant amplitude fatigue tests, but no tests were done concerning the behavior of bonded patches under spectrum loading. Before a decision could be made to repair the C-5A fleet using bonded GLARE® patches, it was necessary to perform spectrum tests to prove the effectiveness of bonded repairs under loads that appear in the actual service life of the aircraft.

The following paragraphs will show the theoretical work behind the qualification process of a bonded repair for the aft crown section of the C-5A Galaxy, as well as the results of the spectrum tests that were performed. The results of this work were also presented at the USAF's ASIP conference in December 1997 in San Antonio, Texas [7.2].

Before spectrum tests could be performed, it was necessary to investigate the effects caused by peak loads. Normally, for an unrepaired cracked structure, peak loads can lead to crack growth retardation. In the case of a bonded repair, several different mechanisms can be of importance. The creation of plastic zones can still occur but on the other hand, peak loads might cause debonds under the patch, resulting in an increased crack growth rate. The overall effect due to these mechanisms was unknown. It was found [7.3] that the effects of peak loads on bonded repairs is similar to the effects of peak loads on unrepaired structures; the crack shows retardation, and no debonds after application of the peak loads were found.

7.4.1 Supplied Data

The data supplied by Kelly AFB is used in an analytical fatigue program to predict crack growth. Data in this particular form is not compatible for use in combination with the MTS® fatigue testing equipment. Also, the Lockheed prediction code can not handle patched cracks. Table 7.1 gives an example of the supplied data.

Flight Type	DSA code	Partial cycles	Minimum stress (psi)	Maximum stress (psi)
1	21	35.73743	4881.302	5916.822
1	21	35.73744	4842.397	5955.727
1	21	35.73743	4794.197	6003.927
1	21	35.73743	4727.005	6071.119
1	21	35.73742	4580.98	6217.142
1	21	7.501760	4263.112	6535.012
1	21	1.000000	3861.912	6936.212
1	21	0.4601240	3297.695	7500.429
1	21	3.8271800E-02	2547.69	8250.429
1	21	1.6042051E-03	1797.69	9000.429

Table 7.1: Spectrum data supplied by Kelly AFB

The data consists of five columns. The first column represents the flight type, followed by a DSA code (Damage Source Assignment, for example taxiing, takeoff, maneuver, etc.). The main incompatibility is the third column, representing partial cycles.

A partial cycle can be non-integer, which cannot exist in a fatigue test (and real-life). The fourth and fifth columns represent the stress combinations, σ_{min} and σ_{max} (psi). Each flight data file consists of approximately 2500 rows (layers). There are 122 flights (21 different types) in one block of 508 flight hours. The total life of a C-5A being is 30,000 hours, 60 blocks need to be constructed to simulate one lifetime. This will result in a life of 7320 flights. In table 7.2, the sequence of the different flight types in a block is given, while table 7.3 shows more information about the different flight types.

nr	ft	nr	ft	nr	ft	nr	ft	nr	ft	nr	ft	nr	ft	nr	ft	nr	Ft	nr	ft	nr	ft
1	1	13	2	25	11	37	7	49	2	61	1	73	4	85	2	97	9	109	2	121	3
2	5	14	3	26	5	38	6	50	5	62	4	74	5	86	11	98	5	110	34	122	25
3	26	15	26	27	26	39	26	51	1	63	26	75	26	87	26	99	26	111	8		
4	2	16	6	28	6	40	40	52	26	64	3	76	1	88	38	100	7	112	26		
5	6	17	4	29	1	41	2	53	4	65	25	77	2	89	25	101	2	113	1		
6	4	18	1	30	4	42	4	54	7	66	1	78	9	90	3	102	6	114	6		
7	1	19	28	31	2	43	25	55	9	67	2	79	3	91	6	103	11	115	7		
8	27	20	25	32	27	44	34	56	1	68	8	80	6	92	31	104	3	116	4		
9	7	21	14	33	9	45	1	57	27	69	7	81	1	93	2	105	4	117	2		
10	9	22	2	34	1	46	10	58	2	70	6	82	27	94	4	106	27	118	1		
11	11	23	1	35	3	47	3	59	6	71	1	83	4	95	35	107	10	119	9		
12	1	24	7	36	11	48	6	60	11	72	11	84	7	96	1	108	25	120	11		

Table 7.2: Sequence of flights in a block, ft = flight type

Flight Type (FY93 Profiles)	Mission Classification Number (Design Missions)	Duration (Minutes)	Number of Flights Per Pass	Number of Hours Per Pass
1	1A	63	18	18.90
2	1B	216	14	51.10
3	1C	493	8	65.73
4	2	168	11	30.80
5	3	491	5	40.92
6	4A	188	11	34.47
7	4B	192	8	25.60
8	4C	186	2	6.20
9	5A	445	6	44.50
10	5B	555	2	18.50
11	5C	443	8	59.07
14	6B	469	1	7.82
25	10A	107	6	10.70
26	10B	224	10	37.33
27	10C	166	5	13.83
28	11A	248	1	4.13
31	11D	210	1	3.50
34	12B	216	2	7.20
35	13A	270	1	4.50
38	14A	261	1	4.35
40	14C	232	1	3.87
			total : 122	

Table 7.3: Information of flights in a block

7.4.2 Spectrum generation method

In the following paragraph, the proposed counting method in order to build a spectrum that can be tested using a fatigue machine will be described in detail. The principle behind this method was approved by Lockheed Martin Aeronautical Systems in Marietta, Georgia in August 1997.

Proposed method
Because of the large amount of data, a computer program, called Generated Spectrum Processor, was developed to generate input data suitable for the MTS® fatigue test equipment. The program adds partial cycles, within set limits, and carries out a "filter-procedure" based on the "identifying-procedure" used during rainflow-counting.

As seen in table 7.1, each layer contains an amount of partial cycles (non-integer, in third column). The program starts reading the data and identifies for each layer σ_{min}, σ_{max} and the number of partial cycles. After the first layer is identified, the program will check whether a particular min-max combination has occurred earlier. If not, this layer is separately placed in the buffer where a so-called bucket, for the partial cycle, is created to store the amount of partial cycles encountered. If the partial cycle occurred earlier, the (partial) amount is added to the same layer (within the buffer tolerance, described later) and stored in the bucket, as long as the cycles originate from the same flight type. This method is called the "Flight method" because it only adds cycles that belong to the same flight type.

After combining the cycles, the program will check whether the partial cycle amount exceeds the bucket size, which can be set to any value. If the partial cycle amount is more than the bucket size, the bucket will be emptied and the min-max combination for that layer in the buffer will be applied. If the partial cycle amount is more than the bucket size, the method will keep subtracting and placing the load combinations in the spectrum until the partial cycle amount is smaller than the bucket size (multiple cycles can be filtered out, see data filtering in section 2.3.5).

A reason for a bucket size higher than one is that high stresses tend to occur in groups caused by, for example, turbulence. These high stress cycles will have larger retardation effects on crack growth when they occur more scattered (bucket size 1). If loads are grouped in sets of more than one load, they will provide conservative crack growth data.

One of the extra options of the program is the adjustable buffer tolerance. This means that, for example, if the buffer tolerance is set at 100 psi, the program will check if there is a load combination in the buffer which differs no more than the buffer tolerance of 100 psi both on σ_{min} and σ_{max}. In this way the total $\Delta\sigma$ will differ no more than twice the buffer tolerance and only partial cycles are added together within the specified range. In this way the buffer tolerance can be seen as a floating bucket related to both σ_{min} and σ_{max}. If the buffer tolerance is set at zero, only partial cycles of load combinations, which are exactly the same, are added. For example bucket: 18-20 ksi, tolerance 1: 17-21 is placed.

Using this method no partial cycles with large differences in $\Delta\sigma$'s are added into one bucket. The reason for the implementation of the adjustable buffer tolerance is that by increasing the tolerance more load combinations can reach a full bucket size depending on the value of the

tolerance. If the buffer tolerance is set at zero, a load combination may never reach the bucket size although many cycles might only be slightly different on both σ_{min} and σ_{max}. After a complete flight has been processed this way, the buffer is stored until the same flight type occurs again. The stored buffer is then used as a start. Therefore, the filling of the bucket continues from the previous flight of that type. This way, each flight of the same type will probably differ slightly. At the end of the construction of a block, all the buffers of the different flight types are saved to be used in the next of the blocks (60 total). All of the 60 blocks will probably be slightly different.

7.4.3 Spectrum data reduction

The next paragraph describes the data reduction method as well as two criteria for deleting cycles. Based on these criteria, different cycles can be removed from the spectrum. By using this data reduction method, testing time can be reduced. Checks must be made to see whether the crack growth rate is equal to the crack growth rate with the unfiltered spectrum.

Data filtering based on rainflow counting

To reduce the data by deleting non-significant cycles, the program has the option to carry out a filter procedure based on the identification of cycles used during rainflow counting. Filtering is done after the cycles are placed via the bucket procedure. There are two situations possible where deleting cycles using this method might be permitted, figure 7.2.

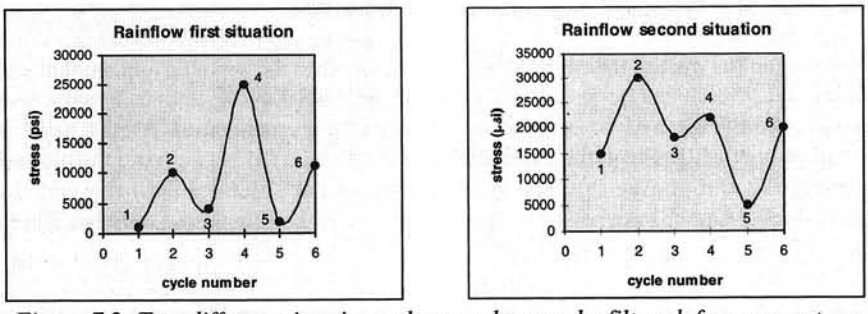

Figure 7.2: Two different situations where cycles can be filtered from a spectrum

Consider the first situation in figure 7.2. Three min-max combinations are considered. The load combinations are 1000-10000 psi (from point 1 to 2), 4000-25000 psi (from point 3 to 4) and 2000-11000 psi (from point 5 to 6). The load step from point 2 to 3 can be deleted if $max_2 <= max_4$ and $min_1 <= min_3$ provided that R ($\sigma_{min3}/\sigma_{max2}$) is over a pre-set value. If so, the step between point 2 and 3 (from 10000 to 4000 psi) is deleted, and the minimum at point 1 is combined with the maximum at point 4 to form the new load combination 1000-25000 psi.

In the second situation in figure 7.2, the cycle from point 3 (20000 psi) to point 4 (25000 psi) can be deleted if $max_4 <= max_2$ and $min_5 <= min_3$. If the R-ratio ($\sigma_{min3}/\sigma_{max4}$) is over the pre-set value, the maximum at point 2 is combined with the minimum at point 5 to form the new load combination 30000-5000 psi.

With this method also diverging and "flat" load sequences can be filtered as long as the R-ratio exceeds the pre-set value. Difficulty in the filter process is to determine the R-ratio which will give a good reduction of cycles (reducing test time), but for which the data after

filtering will still give the same crack growth rate. This seems to be a matter of experience and of preliminary testing. The program has the capability of filtering cycles from a spectrum based on two different criteria.

Discrete filter criterion

The first reduction criterion is called the discrete filter. In the program nine different levels can be set for the filter procedure. By setting the R-ratio levels, cycles with a higher R-value will be filtered from the spectrum. For example if σ_{max} is 10000 psi the R-ratio can be set at a lower level than when σ_{max} is 20000 psi where the cycles are more significant to cause crack growth or creating plasticity at the crack tip. If the R-ratio is set at a lower value, the cycle is more likely to be filtered out. Of course this is less desirable as σ_{max} becomes higher and has more influence on the test results.

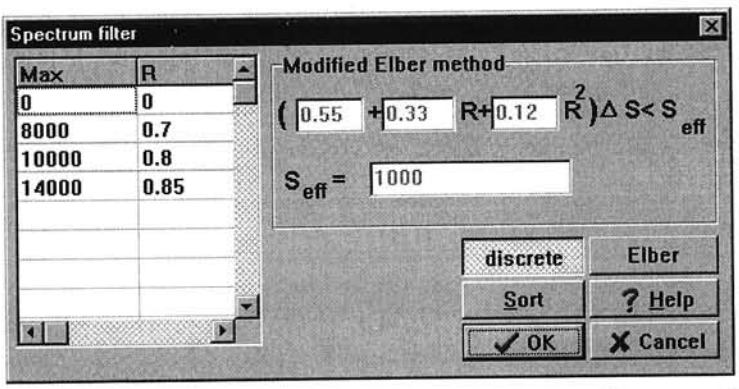

Figure 7.3: Screen capture of the Filter window of the Generated Spectrum Processor

An example of the input for the discrete filter procedure can be seen in the figure 7.3. All cycles (which meet the conditions mentioned at the two rainflow situations in figure 7.2) with σ_{max} between 0 and 8000 psi will be deleted from the data if R is higher than 0. All cycles between 8000 and 10000 psi will be deleted if R is at least 0.7, all cycles with a σ_{max} between 10000 and 14000 psi will be deleted if R is at least 0.8 and all cycles with σ_{max} larger than 14000 psi will be deleted if R is at least 0.85. Up to nine different levels can be specified.

Elber filter criterion

Also shown in figure 7.3, the second criterion is called the modified Elber criterion. This criterion is based on the idea that as long as the crack is still closed due to plasticity in the wake of the crack, a tensile load on the specimen might not be effective. The crack can still be closed, despite a tensile load on the specimen.

Suppose the applied cycle runs from σ_{min} to σ_{max} resulting in $\Delta\sigma$. The stress at which the crack opens will be called the opening stress, σ_{op}. The applied stress cycle is then considered to be reduced from $\Delta\sigma$ to $\Delta\sigma_{eff}$, where $\Delta\sigma_{eff} = \sigma_{max} - \sigma_{op}$. This way, the applied cycle will not be as effective as expected.

For 2024 T3 sheet material, Elber [7.4] originally proposed:

$$U = \frac{\Delta\sigma_{eff}}{\Delta\sigma} = \frac{\Delta K_{eff}}{\Delta K} = 0.5 + 0.4R \qquad (7.1)$$

Schijve showed in [7.5] that the Elber relation would give unrealistic results for negative R values (here, all negative stresses are set to 100 psi due to buckling problems with the specimen geometry used).

Schijve proposed the following equation [7.6]:

$$U = \frac{\Delta\sigma_{eff}}{\Delta\sigma} = \frac{\Delta K_{eff}}{\Delta K} = 0.55 + 0.33R + 0.12R^2 \qquad (7.2)$$

This equation is used for 2024-T3 sheet material without a GLARE® patch. It might be useful for filtering load cycles from spectrum data in more situations. Since the equation is empirical, the exact form of the equation has to be determined by verifying it with test results representing the configuration tested (materials, patches, bonding etc.). The equation can be rewritten to:

$$(0.55 + 0.33R + 0.12R^2)\Delta\sigma = \Delta\sigma_{eff} \qquad (7.3)$$

By defining a maximum $\Delta\sigma_{eff}$, all cycles (which satisfy the conditions mentioned at the two rainflow situations in figure 7.2) of which the calculated $\Delta\sigma_{eff}$ is lower than the defined $\Delta\sigma_{eff}$, will be filtered out of the spectrum.

As will be shown later, filtering with the modified Elber criterion is not as selective as the discrete criterion.

7.4.4 Truncation of spectrum

Truncation of high loads may have a large effect on the fatigue life of a specimen. In a spectrum, it is possible that exceptionally high peak loads incidentally occur which will reduce crack growth, even in patched specimens. Not all aircraft in service will encounter these high loads.

Due to the fact that high peak loads cause plasticity at the crack tip, this can cause a significant retardation in crack growth. To get conservative results when testing specimens, it is necessary to truncate infrequently occurring high loads.

In [7.7], it is suggested that in order to get conservative results, a spectrum should be truncated at a load level which will be exceeded fewer than an average of ten times in the life of the aircraft. Although this is an arbitrary limit, it seems to be accepted in most cases, Airbus uses this same limit.

The first results of the Generated Spectrum Processor show that a filtered life built with the Flight method does not contain these exceptionally high loads. Higher loads, that occur in the spectrum, appear in larger quantities. For that reason there will be no truncation for the time

being. By setting an upper limit of 40000 psi, no truncation will take place because of the fact that all occurring loads in the spectrum data are significantly lower.

Negative loads have to be avoided during testing to keep the unsupported specimen from buckling resulting in damage. In the full-scale aircraft structure the structure will be stiffened and will be able to carry compressive loads. To avoid the (quite rare) negative loads on the specimens during testing, a lower limit is defined after the data has been filtered. Negative loads will be set to 100 psi to retain as much of the original $\Delta\sigma$ as possible.

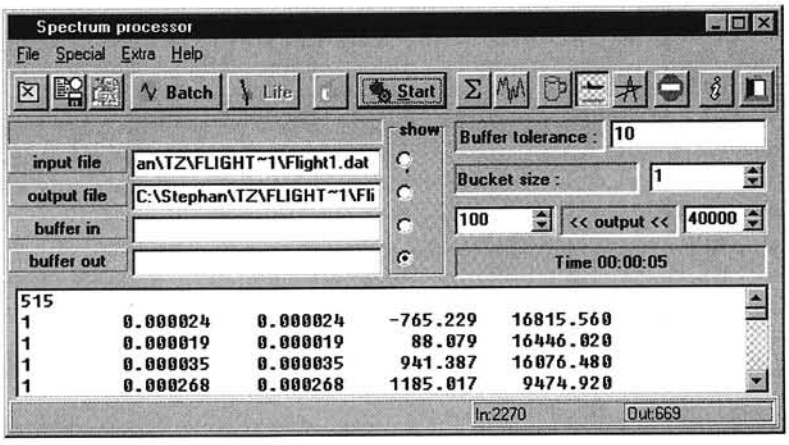

Figure 7.4: Screencapture of Generated Spectrum Processor

More about the data reduction and filter criteria can be found in [7.3]. Also in this report are results of initial spectrum tests on unpatched panels with filtered and unfiltered spectra.

7.4.5 Spectrum tests

Using two different C-5A spectra, one filtered and one unfiltered, two patched and two unpatched 7075-T6 panels were tested. Sixty blocks had to be tested to simulate one C-5A life. The tests performed are given in table 7.4. The GLARE® patches were 60 x 50 mm. The patched panels were 1.0 mm thick, 180 mm wide and 436.5 mm long. The unpatched panels were 152.4 mm (6 inches) wide and 400 mm long, the pre-crack is 25 mm.

Specimen #	Spectrum type	Pre-crack level (MPa)	Patch
01	Filtered	60-6	none
06	Unfiltered	60-6	none
S3	Filtered	60-6	GLARE2
S6	Unfiltered	60-6	GLARE2

Table 7.4: Spectrum test program

Figure 7.5 shows the crack growth curves for the four specimens. It is clear how effective the patches are in reducing crack growth under realistic crown fuselage spectra. The curves for the patched specimens are almost horizontal, implying the extremely low crack growth rates. It can also be seen that the difference between the two different spectra is insignificant for crack growth under the patches. It is no problem for the repair to withstand one full C-5A life. If the

patched structure is assumed to be non-inspectable, the minimum required life is twice the remaining life of the aircraft. Assuming that the C-5A's are at 75 percent of their life, only half a lifetime has to be proven. The patched cracks have this capability. Debonding is of no concern for correctly applied patches, loaded under realistic loading conditions. C-scans of the two patched specimens did not show any signs of debonding.

As can be concluded from figure 7.5, for crack growth under a bonded repair smaller cycles are less important than for an unpatched specimen. The cycles that were filtered out were apparently too small to cause any crack growth under the patch. The patch reduces ΔK so much that these small cycles are below the threshold value for fatigue growth.

Filtering small cycles out of the spectrum can be very beneficial for saving testing time. The filtered spectrum could be tested in 10 percent of the time of the unfiltered spectrum, resulting in the same crack growth. It must be said that thorough checks have to be made to verify that the filtered spectrum results in the same crack growth results. If this is neglected, the test results can be invalid.

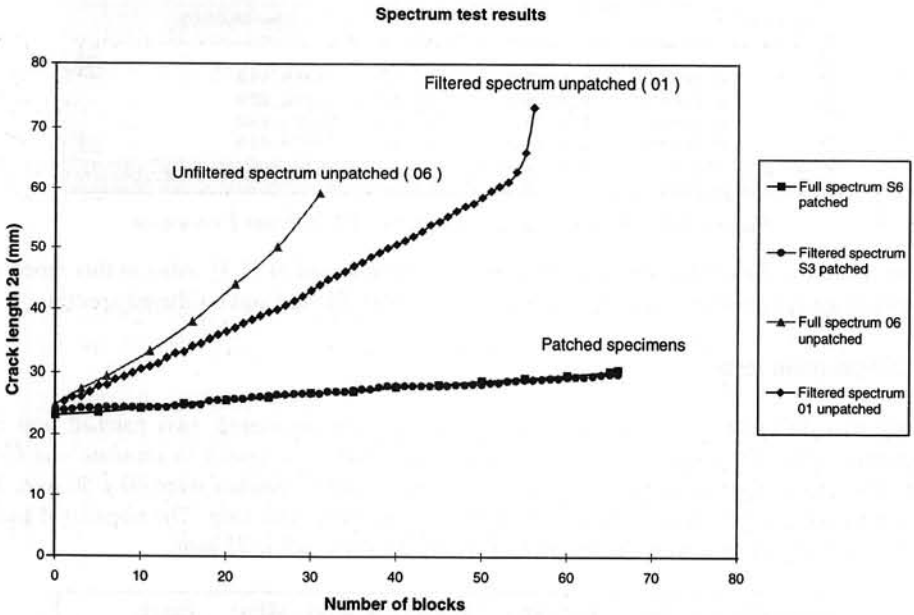

Figure 7.5: Crack growth curves for unpatched and patched 7075 specimens under spectrum loading [7.2/7.8]

7.5 Conclusions

From this chapter it can be concluded that:

- A computer program has been made to be able to translate spectrum data for a crack growth prediction code into data that is suited for usage on a fatigue machine.
- Smaller cycles are less important for crack growth under a bonded repair than for an unpatched specimen. The cycles that were filtered out were apparently too small to cause any crack growth under the patch. The patch reduces ΔK so much that these small cycles are below the threshold value for fatigue growth.
- It is clear how effective the patches are in reducing crack growth under realistic crown fuselage spectra. The curves for the patched specimens are almost horizontal, implying the extremely low crack growth rates. It can also be seen that the difference between the two different spectra is insignificant for crack growth under the patches.
- It is no problem for the repair to withstand one full C-5A life. If the patched structure is assumed to be non-inspectable, the minimum required life is twice the remaining life of the aircraft. Assuming that the C-5A's are at 75 percent of their life, only half a lifetime has to be proven. The repairs have this capability.
- Debonding is of no concern for correctly applied patches, loaded under realistic loading conditions. C-scans of the two patched specimens did not show any signs of debonding.
- Filtering small cycles out of the spectrum can be very beneficial for saving testing time. The filtered spectrum could be tested in 10 percent of the time of the unfiltered spectrum, resulting in the same crack growth. It must be said that thorough checks have to be made to verify that the filtered spectrum results in the same crack growth results. If this is neglected, the test results can be invalid.

[7.1] Fredell, R.S., Guijt, C.B., USAFA, Conley, D., WL/FIBEC, Knighton, S., Collas, E., SA-ALC LADD, *Design Development of a Bonded Fuselage Repair for the C-5A*, US Air Force Document.

[7.2] Verhoeven, S., Guijt, C.B., Vlot, A., Delft University of Technology/United States Air Force Academy, Colorado, Collas, E., San Antonio ALC, *Qualification of a Bonded Repair to C-5A Fuselage Cracking under Spectrum Fatigue Loading*, 1997 USAF Aircraft Structural Integrity Program Conference, San Antonio, Texas, December 1997.

[7.3] Verhoeven, S., *Preparation of the Spectrum Testing of Bonded GLARE Repairs for the C-5A Galaxy, a study of the interaction effects of peak loads on bonded repairs and a proposal for the modification of C-5A aft crown spectrum data*, TZ Report, Delft University of Technology, The Netherlands, June 1997.

[7.4] Elber, W., *The significance of crack closure.* ASTM STP 486, 1971, pp. 230-242.

[7.5] Schijve, J., *The stress ratio effect on fatigue crack growth in 2024-T3 Alclad and the relation to crack closure*, Delft University of Technology, Memorandum M-336, August 1979.

[7.6] Schijve, J., *Some formulas for the crack opening stress level*, Delft University of Technology, Memorandum M-368, April 1980.

[7.7] Schijve, J., *The significance of flight-simulation fatigue tests*, Delft University of Technology, Report LR-466, June 1985.

[7.8] Verhoeven, S., *In-Service Effects on Crack Growth under Bonded Composite Repairs*, Master Thesis, Delft University of Technology, The Netherlands, July 21st, 1998.

Series 01: Aerodynamics

01. F. Motallebi, 'Prediction of Mean Flow Data for Adiabatic 2-D Compressible Turbulent Boundary Layers'
1997 / VI + 90 pages / ISBN 90-407-1564-5
02. P.E. Skåre, 'Flow Measurements for an Afterbody in a Vertical Wind Tunnel'
1997 / XIV + 98 pages / ISBN 90-407-1565-3
03. B.W. van Oudheusden, 'Investigation of Large-Amplitude 1-DOF Rotational Galloping'
1998 / IV + 100 pages / ISBN 90-407-1566-1
04. E.M. Houtman / W.J. Bannink / B.H. Timmerman, 'Experimental and Computational Study of a Blunt Cylinder-Flare Model in High Supersonic Flow'
1998 / VIII + 40 pages / ISBN 90-407-1567-X
05. G.J.D. Zondervan, 'A Review of Propeller Modelling Techniques Based on Euler Methods'
1998 / IV + 84 pages / ISBN 90-407-1568-8
06. M.J. Tummers / D.M. Passchier, 'Spectral Analysis of Individual Realization LDA Data'
1998 / VIII + 36 pages / ISBN 90-407-1569-6
07. P.J.J. Moeleker, 'Linear Temporal Stability Analysis'
1998 / VI + 74 pages / ISBN 90-407-1570-X
08. B.W. van Oudheusden, 'Galloping Behaviour of an Aeroelastic Oscillator with Two Degrees of Freedom'
1998 / IV + 128 pages / ISBN 90-407-1571-8
09. R. Mayer, 'Orientation on Quantitative IR-thermografy in Wall-shear Stress Measurements'
1998 / XII + 108 pages / ISBN 90-407-1572-6
10. K.J.A. Westin / R.A.W.M. Henkes, 'Prediction of Bypass Transition with Differential Reynolds Stress Models'
1998 / VI + 78 pages / ISBN 90-407-1573-4
11. J.L.M. Nijholt, 'Design of a Michelson Interferometer for Quantitative Refraction Index Profile Measurements'
1998 / 60 pages / ISBN 90-407-1574-2
12. R.A.W.M. Henkes / J.L. van Ingen, 'Overview of Stability and Transition in External Aerodynamics'
1998 / IV + 48 pages / ISBN 90-407-1575-0
13. R.A.W.M. Henkes, 'Overview of Turbulence Models for External Aerodynamics'
1998 / IV + 40 pages / ISBN 90-407-1576-9
14. G. Schouten, 'The Two-Dimensional Soundfield of a Vortex Moving Around the Sharp Edge of a Half-Plane'
1998 / VI + 26 pages / ISBN 90-407-1730-3
15. M.M.J. Schoones / W.J. Bannink, 'Base Flow and Exhaust Plume Interaction. Part 1: Experimental Study'
1998 / VIII + 64 pages / ISBN 90-407-1747-8

16. M.M.J. Schoones / E.M. Houtman, 'Base Flow and Exhaust Plume Interaction. Part 2: Computational Study'
1998 / VIII + 86 pages / ISBN 90-407-1748-6

Series 02: Flight Mechanics

01. E. Obert, 'A Method for the Determination of the Effect of Propeller Slipstream on a Static Longitudinal Stability and Control of Multi-engined Aircraft'
1997 / IV + 276 pages / ISBN 90-407-1577-7
02. C. Bill / F. van Dalen / A. Rothwell, 'Aircraft Design and Analysis System (ADAS)'
1997 / X + 222 pages / ISBN 90-407-1578-5
03. E. Torenbeek, 'Optimum Cruise Performance of Subsonic Transport Aircraft'
1998 / X + 66 pages / ISBN 90-407-1579-3

Series 03: Control and Simulation

01. J.C. Gibson, 'The Definition, Understanding and Design of Aircraft Handling Qualities'
1997 / X + 162 pages / ISBN 90-407-1580-7
02. E.A. Lomonova, 'A System Look at Electromechanical Actuation for Primary Flight Control'
1997 / XIV + 110 pages / ISBN 90-407-1581-5
03. C.A.A.M. van der Linden, 'DASMAT-Delft University Aircraft Simulation Model and Analysis Tool. A Matlab/Simulink Environment for Flight Dynamics and Control Analysis'
1998 / XII + 220 pages / ISBN 90-407-1582-3
04. S.K. Advani, 'The Kinematic Design of Flight Simulator Motion-Bases'
1998 / XVIII + 244 pages / ISBN 90-407-1671-4
05. J.M. Maciejowski, 'Predictive Control. A Lecture Course Given in the Aerospace Engineering Faculty TU Delft'
1998 / XII + 156 pages / ISBN 90-407-1714-1

Series 05: Aerospace Structures and Computional Mechanics

01. A.J. van Eekelen, 'Review and Selection of Methods for Structural Reliability Analysis'
1997 / XIV + 50 pages / ISBN 90-407-1583-1
02. M.E. Heerschap, 'User's Manual for the Computer Program Cufus. Quick Design Procedure for a CUt-out in a FUSelage version 1.0'
1997 / VIII + 144 pages / ISBN 90-407-1584-X
03. C. Wohlever, 'A Preliminary Evaluation of the B2000 Nonlinear Shell Element Q8N.SM'
1998 / IV + 44 pages / ISBN 90-407-1585-8
04. L. Gunawan, 'Imperfections Measurements of a Perfect Shell with Specially Designed Equipment (UNIVIMP)
1998 / VIII + 52 pages / ISBN 90-407-1586-6

Series 07: Aerospace Materials

01. A. Vašek / J. Schijve, 'Residual Strenght of Cracked 7075 T6 Al-alloy Sheets under High Loading Rates'
1997 / VI + 70 pages / ISBN 90-407-1587-4
02. I. Kunes, 'FEM Modelling of Elastoplastic Stress and Strain Field in Centre-cracked Plate'
1997 / IV + 32 pages / ISBN 90-407-1588-2
03. K. Verolme, 'The Initial Buckling Behavior of Flat and Curved Fiber Metal Laminate Panels'
1998 / VIII + 60 pages / ISBN 90-407-1589-0
04. P.W.C. Provó Kluit, 'A New Method of Impregnating PEI Sheets for the *In-Situ* Foaming of Sandwiches'
1998 / IV + 28 pages / ISBN 90-407-1590-4
05. A. Vlot / T. Soerjanto / I. Yeri / J.A. Schelling, 'Residual Thermal Stresses around Bonded Fibre Metal Laminate Repair Patches on an Aircraft Fuselage'
1998 / IV + 24 pages / ISBN 90-407-1591-2
06. A. Vlot, 'High Strain Rate Tests on Fibre Metal Laminates'
1998 / IV + 44 pages / ISBN 90-407-1592-0
07. S. Fawaz, 'Application of the Virtual Crack Closure Technique to Calculate Stress Intensity Factors for Through Cracks with an Oblique Elliptical Crack Front'
1998 / VIII + 56 pages / ISBN 90-407-1593-9
08. J. Schijve, 'Fatigue Specimens for Sheet and Plate Material'
1998 / VI + 18 pages / ISBN 90-407-1594-7
09. J. Schijve, 'The Significance of Fractography for Investigations of Fatigue Crack Growth under Variable-Amplitude Loading'
1998 / IV + 34 pages / ISBN 90-407-1716-8

10. M.J.L. van Tooren / Z.C. Roza, 'Finite Difference Methods for Stress Analysis of Adhesive Bonded Joints. The Design of a MATLAB Adhesive Toolbox'
1998 / VIII + 94 pages / ISBN 90-407-1717-6
11. A. Vlot / S. Verhoeven / P.J.M. Nijssen 'Bonded Repairs for Aircraft Fuselages'
1998 / VIII + 82 pages / ISBN 90-407-1804-0

Series 08: Astrodynamics and Satellite Systems

01. E. Mooij, 'The Motion of a Vehicle in a Planetary Atmosphere'
1997 / XVI + 156 pages / ISBN 90-407-1595-5
02. G.A. Bartels, 'GPS-Antenna Phase Center Measurements Performed in an Anechoic Chamber'
1997 / X + 70 pages / ISBN 90-407-1596-3
03. E. Mooij, 'Linear Quadratic Regulator Design for an Unpowered, Winged Re-entry Vehicle'
1998 / X + 154 pages / ISBN 90-407-1597-1

3021909

Today's economic restrictions force operators to use their aircraft longer than intended by their designers. Fatigue problems become an important topic in the maintenance of these aircraft. These so-called "aging aircraft" need safe, damage tolerant and cost-effective repairs.

Instead of using riveted repairs, bonded repairs can be a more viable solution. Compared to mechanically fastening such as riveting or bolting, adhesively bonding provides a more uniform and efficient load transfer into the patch and can reduce the risk of high stress concentrations. Repair materials for metallic structures are for example carbon- and boron-reinforced epoxy. These materials have some disadvantages, such as a large mismatch in thermal expansion coefficient (CTE). The fiber metal laminate GLARE® does not have this large CTE mismatch, therefore high residual stresses due to the curing process and operating temperature are prevented.

This report will give an overview of the bonded repair work that has been done over the last few years by the Faculty of Aerospace Engineering of Delft University of Technology, in cooperation with the Center for Aircraft Structural Life Extension at the United States Air Force Academy in Colorado Springs.

The first chapters will give some general information about design, analysis, processes and materials used in bonded repairs. After these introductory chapters the bonded repair analysis program CalcuRep®, an analytical program well suited for in-field usage by maintenance personnel, is described. The results of several calculations of stress intensity factors and stresses in the periphery of bonded patches are given. Tests were performed with repairs subjected to realistic in-service conditions. The effect of debonds was investigated and it was found that artificial debonds can have an effect on crack growth, although limited. The influence of the ground-air-ground temperature cycle was investigated. Tests showed no effect for specimens with boron and GLARE® patches. Specimens with these same patches that were loaded in fatigue at low temperatures, simulating low temperatures experienced at cruising altitude, showed significantly lower crack growth rates when tested at -40°C. Finally, the application and qualification of a bonded GLARE® repair on a C-5A Galaxy cargo aircraft is described. Tests were performed to investigate the crack growth and debond behavior of bonded repairs under variable amplitude fatigue loading and showed that bonded repairs are very effective in slowing down crack growth under realistic fuselage spectra and that debonding was of no concern.

ISBN 90-407-1804-0
9 789040 718044

DELFT AEROSPACE
ENGINEERING & TECHNOLOGY